Universiteit Utrecht

Faculteit Bètawetenschappen

Conductivity of a charge-regulated Boron-Nitride nanotube

Bachelor Thesis

B. Boer

Natuur- en Sterrenkunde

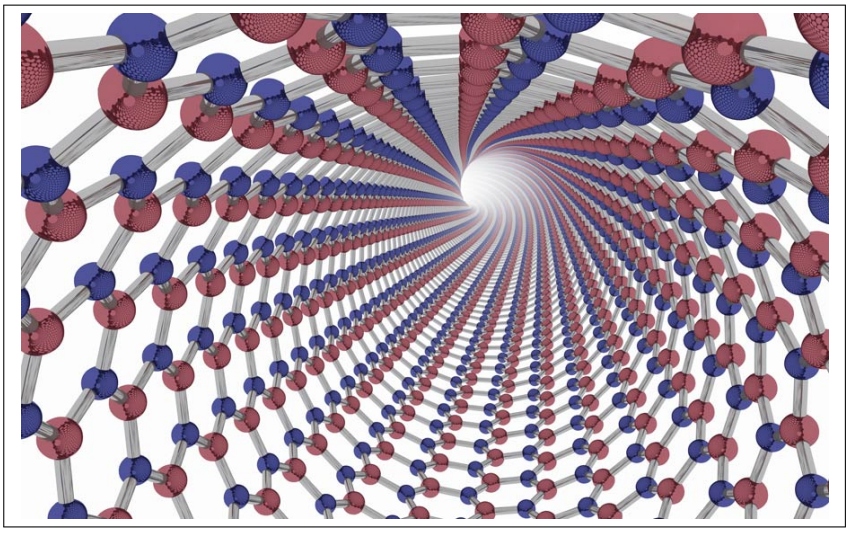

Supervisors:

Prof. Dr. R.H.H.G. van Roij First Supervisor
Institute for Theoretical Physics, Utrecht

MSc B.L. Werkhoven Second Supervisor
Institute for Theoretical Physics, Utrecht

Dr. J. de Graaf Third Supervisor
Institute for Theoretical Physics, Utrecht

June 12, 2018

Abstract

In this thesis we investigate the physical properties of a Boron-Nitride NanoTube(BNNT), in particular the electric conductivity of the nanotube. The nanotube connects two reservoirs of different salt concentration. We applied a concentration gradient of Na^+ and Cl^- in the nanotube and studied whether we could compare the conductivity of the nanotube to the conductivity of a conducting wire. The method of the research was a simulation with the finite element method in COMSOL. We found a surface conductivity constant $g_s = 2.3 \cdot 10^3$ S/m^2 and a bulk conductivity constant $g_b = -1.8 \cdot 10^2$ S/m for a BNNT with a regulated surface charge and a pH value of 5.5, in the regime where the radius of the tube is larger then the Debye length. For a radius smaller then the Debye length g_b was varying too much to make a reliable prediction.

Contents

1 Introduction

Due to the emission of greenhouse-gases and exploitation of the earth, we are currently dealing with climate change. With the growing human population, the total energy demand is increasing. This energy has to be produced from sustainable energy sources to stop the continued pollution of the environment. Most commonly known sustainable energy sources are: sunlight, wind and energy from barrages. A relatively new and unknown form of sustainable energy is "blue" energy, which is currently tested in The Netherlands at the Afsluitdijk, which is run by a company named REDstack[1]. Blue energy is energy that is produced by tapping from the salinity gradient between seawater (with a high salt concentration) and river water (with a lower salt concentration). This is done by using selective membranes that enable ions to move through nanopores and thereby create a potential difference. This potential difference is used to produce energy. In this research a single nanotube is studied in which ions are transported from a reservoir of seawater to a reservoir of river water. The nanotube which is studied is made of Boron-Nitride which has a high surface charge, this high surface charge causes a very effective ion transport[2]. To describe this surface charge realisticly we used a charge regulation model, in which the surface charge depends on the ion concentration. When blue energy is generated it is the goal of energy producing companies to maximize the efficiency. A measure of the efficiency is the conductivity of the nanotube, because when the conductivity is maximized the current and therefore the energy production are also maximized. In this thesis we study the conductivity of the charge-regulated Boron-Nitride nanotube which is exposed to a salt concentration gradient and investigate whether we can compare it with a conducting wire. Thus the research question can be formulated as: How does the radius of a Boron-Nitride nanotube affect the conductivity? To answer this question we first discuss the relevant theory in Sec. 2, then we describe the way our simulations are done in Sec. 3. Thereafter the results are given in Sec. 4. Section 5 concludes this thesis.

2 Theory

2.1 Blue energy

2.1.1 Water

Before we discuss what blue energy is we must first consider what the components are of the different kinds of water we use. In Table 1 the components of seawater are shown[3]. We assume that river water consists only of H_2O, while it actually has a salt concentration which is about 25 times smaller then seawater, however for these calculations we choose to neglect this (the other components of river water are negligible and do not play a role for describing our system). Furthermore we assume that seawater only consists of a mixture of H_2O, Cl^- and Na^+ for practical purposes in this thesis. These assumptions are justified if one realises that in Table 1 the concentration of other molecules and ions in the sea are an order in magnitude lower than these three species. Moreover, the river water composition is very dependent on which river is concerned. Therefore it is more practical to consider pure water and keeping in mind that for real applications the outcomes of this research need to be considered as an approximation. In the following part of this thesis river water will also be called fresh water, seawater will also be called the saline solution and after mixing the term brackish water will be used for the mixed water.

Component	Concentration (in mol/kg)
H_2O	53.6
Cl^-	0.549
Na^+	0.469
Mg^{2+}	0.0528
SO_4^{2-}	0.0282
Ca^{2+}	0.0103
K^+	0.0102

Table 1: The composition of seawater[3].

Volume fractions	x_{H_2O}	x_{Cl^-}	x_{Na^+}
Saline water	0.981	0.010	0.009
Fresh water	1	0	0
Brackish water	0.991	0.005	0.004

Table 2: The volume fractions of components of seawater and their respective entropy of mixing. Calculated from Table 1.

2.1.2 The origin of blue energy

When saline water is mixed with fresh water the free energy of the system will decrease, this is a result of the increased entropy. We are interested in the amount of energy that can be produced from mixing a litre of sea water with a litre fresh water. Therefore we consider the Helmholtz free energy $F = U - TS$, where U is the internal energy, T the temperature and S the entropy. We can write the $S = k_B \log \Omega$, where k_B is the Boltzmann constant and Ω the number of microstates. The number of microstates Ω is equal to $\frac{N!}{N_{H_2O}! N_{Na^+}! N_{Cl^-}!}$, where N is the total number of particles and N_i is the number of particles of specie i. Combining these formulas and using the Stirling approximation ($\log x! \approx x \log x - x$) gives

$$F = U - k_B T[N \log N - N - (\sum_{i=1}^{3} N_i \log N_i - N_i)], \tag{2.1}$$

$$= U + N k_B T \sum_{i=1}^{3} x_i \log x_i. \tag{2.2}$$

In which $x_i = \frac{N_i}{N}$ is the particle fraction of species i. Thus when the entropy S, which is substituted in Eq. (2.2) changes, the Helmholtz free energy F changes as well. In Fig. 1 a schematic overview of the mixing

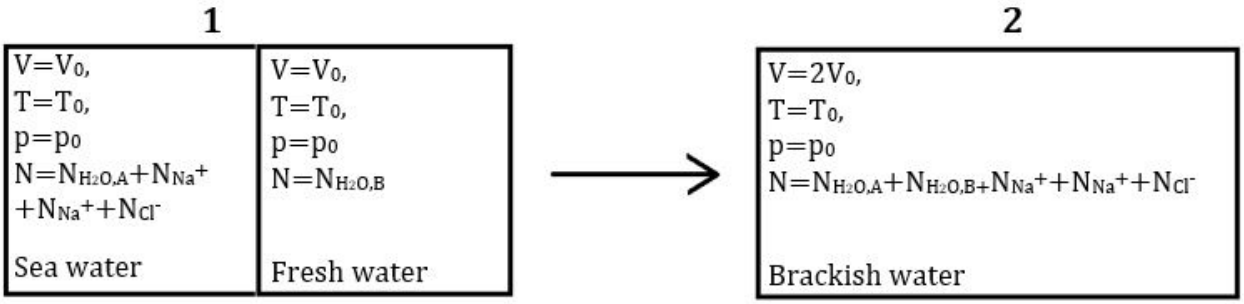

Figure 1: Schematic overview of the mixing of river water with seawater, which results in brackish water.

process is given. Due to the fact that the total system, the fresh water system together with the sea water system, has a constant internal energy U the change in Helmholtz free energy ΔF is written as

$$\Delta F = F_b - F_s - F_f, \tag{2.3}$$

$$= (N_s + N_f) k_B T \sum_{i=1,b}^{3} x_i \log x_i - N_s k_B T \sum_{i=1,s}^{3} x_i \log x_i. \tag{2.4}$$

Where we substituted Eq. (2.2) for each component. The subscripts b, s and f refer to brackish, sea and fresh water respectively[5]. The quantities $N_s = N_{H_2O,A} + N_{Na^+} + N_{Cl^-}$ and $N_f = N_{H_2O,B}$ are the number of particles in sea water and fresh water, respectively. Note that the sum over the fresh water components vanishes because this has only one component. With Eq. (2.4) and Table 1 we can now calculate the available energy per unit volume. We mix one litre of saline water with one litre of fresh water (pure H_2O). From this we calculate the work per unit volume for water of $T = 283$ degrees Kelvin (the average seawater temperature in The Netherlands [6]) $\Rightarrow \Delta F/V \approx 1$ MJ m^{-3}. How this energy is gained from this entropy change will be explained in the following sections.

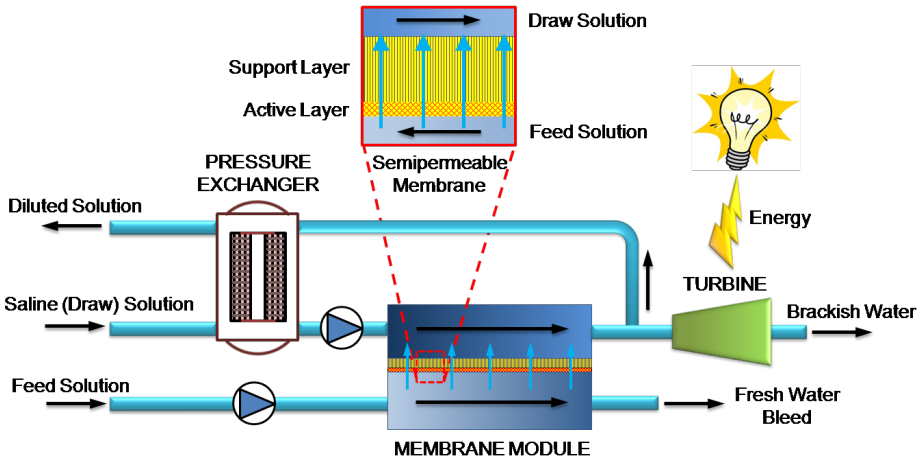

Figure 2: Schematic overview of pressure-retarded osmosis. In the membrane module water molecules travel through the semi-permeable membrane from the feed solution(fresh water with a low salt concentration) to the saline solution. Due to this osmosis the pressure in the upper part of the module increases. With the turbine this pressure difference is used to produce electricity[7].

2.1.3 Pressure retarded osmosis

One way to produce energy by mixing salt water and fresh water is to use a membrane that connects two reservoirs of different salinity. The reservoirs are connected with a semi-permeable membrane and therefore the system undergoes osmosis, which means that there will be an induced water flow from the reservoir with low salinity (river water) to the reservoir with the higher salinity (seawater)[7]. Hence the pressure of the salt water increases due to the flow of H_2O, because the volumes of the reservoirs remain the same. From this pressure difference energy can be produced with a turbine. A schematic overview of this production type is given in Fig. 2.

2.1.4 Reverse electro-dialysis

Another way to produce energy from the mixing of seawater and river water is reverse electro-dialysis, this is logically the reversal of electro-dialysis. In electro-dialysis water is desalinated by applying an electric field, where reverse electro-dialysis uses the mixing of ions to generate an electric field. This electric field is generated by diffusion of ions through semi-permeable membranes. Due to the selective membranes at one side of the membrane there will be a majority of negatively charged ions, while on the other side there will be a majority of positively charged particles, see Fig. 3. Using redox-reactions electrons can move from the anode in the negatively charged bath to the cathode in the positively charged bath. This current van be used to produce energy, which we call blue energy.

2.2 Nanotube

In the previous section we explained how reverse electro-dialysis works. Now we are zooming in on the semi-permeable membrane for positively charged ions. This membrane consists of a lot of nanopores, where Na^+-ions travel through. The system of a nanotube with transported ions is shown and explained in Fig. 4. In this thesis we will discuss the physical properties of a single nanotube. This is slightly different from a nanopore due to the fact that the nanotube has a smaller radius than the average radius of nanopores in membranes which are commonly used. The nanotube connects two reservoirs(baths), one with seawater and one with river water as we have seen in Fig. 3. The surface of the nanotube is negatively charged, therefore only Na^+-ions can travel through. When this nanotube is made of Boron-Nitride the surface charge can be relatively high (1 Cm^{-2}) for certain values of pH[2].

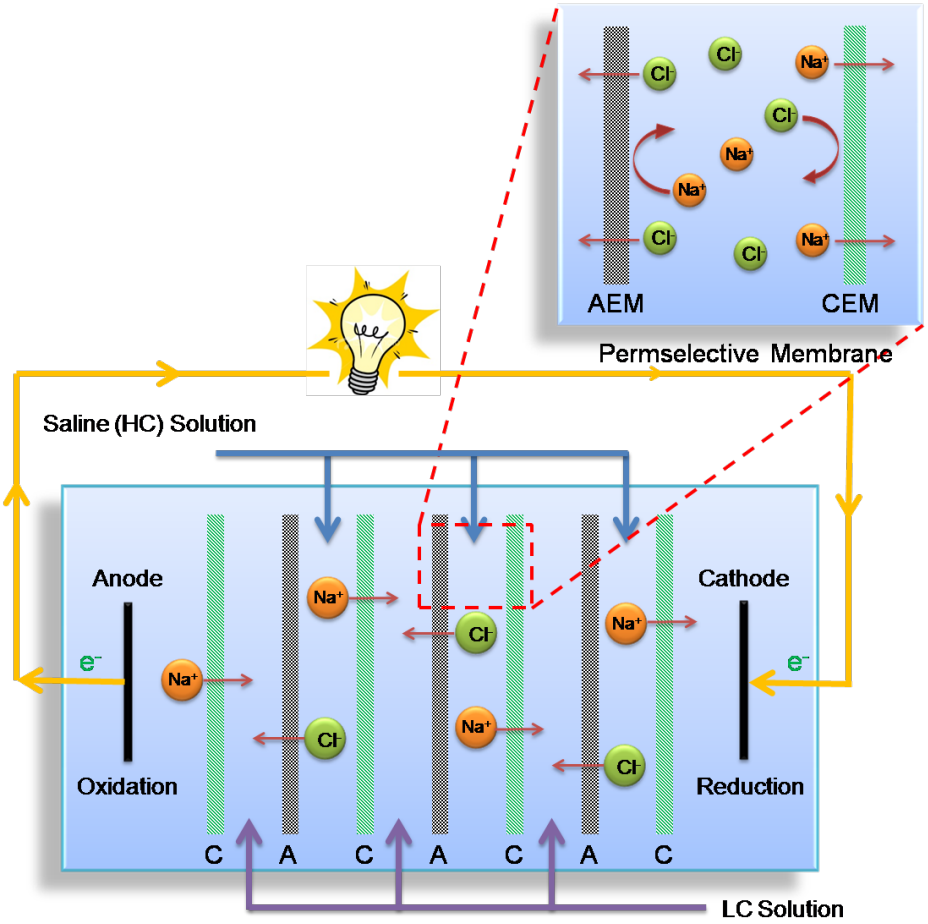

Figure 3: Schematic overview of reverse electro-dialysis. From the saline solution (High Concentration of salts(HC)), the salts diffuse through selective membranes to the dilute water (Low Concentration of salts(LC)). Due to the selectivity of the membranes an electric potential is induced between the anode and the cathode. With reduction-oxidation reactions electrons are absorbed at the anode and emitted at the cathode, due to these reactions a current is generated. This current can be used for power devices[7].

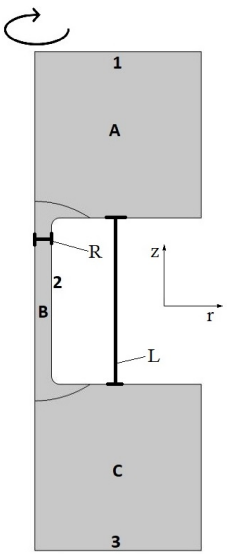

Figure 4: In this figure a schematic overview of the geometry is shown. The geometry consists of 3 parts: Bath A, bath C and the nanotube B. Note that the entire geometry has to be rotated in order to get an axis-symmetric 3D-volume.
The capitals in the figure correspond to the volume in which the capital is located. Bath A is filled with seawater, which consists of H_2O, Na^+ and Cl^-, see Sec. 2.1.1. Bath C is filled with river water, which consist only of H_2O. The nanotube B is the tube through which the ions diffuse from A to C, this tube has a length(L) of 400 nm and a radius(R) of 40 nm.
The numbers in the figure correspond to the edge nearby. Edge 1 is responsible for the inlet of seawater, we define that at this edge the concentration of Na^+ and Cl^- remains constant, because we assume that this bath is infinite. Edge 3 is responsible for the outlet of the flow. Edge 2 is the surface of the nanotube, due to charge generation processes the surface of the nanotube becomes charged, we define σ to be the surface charge density.
The curved lines that divide parts A and B & B and C, are the boundaries of the mesh for each region. The mesh is split into regions, because the nanotube needs more meshpoints (points where the differential equations are solved).
The coordinate axes indicate the radial(r) and axial(z) direction.

2.3 Equations to describe the fluid

2.3.1 Navier-Stokes equation

The Navier-Stokes equation is obtained by applying Newton's second law to a small volume. We use Newtons second law, $m\mathbf{a} = \sum \mathbf{F}$, where m is the mass of the volume, $\mathbf{a}$ is the acceleration and $\sum \mathbf{F}$ is the sum of all the forces. This can be rewritten as $\rho\mathbf{a} = \sum \mathbf{f}$, where ρ is the mass density and $\mathbf{f}$ is the sum of all the forces per unit volume. Using the material derivative (F.15) derived in App. F.2, the continuity equation, which is derived in App. F.1 for an incompressible fluid($\frac{\partial \rho}{\partial t} = 0$) and knowledge of which forces work on the volume the following equations are obtained. For a complete derivation of the force terms in the Navier-Stokes equation we recommend Ref. [8], that we follow closely here. We write

$$\rho(\frac{\partial \mathbf{u}}{\partial t} + \mathbf{u} \cdot \nabla \mathbf{u}) = -\nabla p + \eta \nabla^2 \mathbf{u} + \mathbf{f}; \qquad \nabla \cdot \mathbf{u} = 0. \tag{2.5}$$

In this equation $-\nabla p$ is the pressure gradient, $\eta \nabla^2 \mathbf{u}$ is the friction force due to velocity gradients with η the viscosity and $\mathbf{f}$ all remaining body forces. If the friction term is very high compared to the inertia term $\rho \mathbf{u} \cdot \nabla \mathbf{u}$, the inertia term can be neglected. To check whether this assumption is accurate the Reynolds number is introduced: $\mathrm{Re} = \frac{|\rho \mathbf{u} \cdot \nabla \mathbf{u}|}{|\eta \nabla^2 \mathbf{u}|} = \frac{\rho U L}{\eta}$, where U is the typical velocity and L the typical length scale. The condition $\nabla \cdot \mathbf{u} = 0$ indicates that the fluid is incompressible. For $\mathrm{Re} \ll 1$ the inertia term can be neglected. When describing a fluid at nano-scales often $\mathrm{Re} \ll 1$, therefore the inertia term can be neglected. Hence the Navier-Stokes equation (2.5) reduces to the Stokes equation,

$$\rho \frac{\partial \mathbf{u}}{\partial t} = -\nabla p + \eta \nabla^2 \mathbf{u} + \mathbf{f}; \qquad \nabla \cdot \mathbf{u} = 0. \tag{2.6}$$

The Stokes equation describes the motion of a fluid for small Reynolds number.

2.3.2 Equation fluid nanotube

The relevant equation for describing the flow of the fluid is the Stokes equation (2.6), where we add and subtract some terms. If the flow is stationary, we can say $\frac{\partial \mathbf{u}}{\partial t} = 0$. We will assume a stationary state throughout the thesis. Here we will focus on a solution of charged particles which are not locally neutral throughout space, because the surface charge generates an electric field in the nanotube, therefore $\mathbf{f} = Q\mathbf{E} =$

$-\epsilon_0\epsilon_r(\nabla^2\psi)\nabla\psi$, where in this case the Q is the charge, note that we used the Poisson equation (2.8). Due to these two implementations the Stokes equation (2.6) becomes

$$\eta\nabla^2\mathbf{u} = \nabla p + \epsilon_0\epsilon_r(\nabla^2\psi)\nabla\psi; \qquad \nabla\cdot\mathbf{u} = 0. \tag{2.7}$$

This equation is solved by iterations in COMSOL, the program that we use to solve the differential equations of flow together with the equations that apply the movement of ions in the fluid, which will be discussed in the following section.

2.4 Equations to describe the ions in the fluid

2.4.1 Poisson equation

To describe the electrostatics, of the by approximation homogeneous dielectric medium, we derive the Poisson equation. We use Gauss's Law: $\nabla\cdot\mathbf{D} = Q_f$, where $\mathbf{D}$ is the electric displacement and Q_f is the free charge density. The equation for the electric displacement is: $\mathbf{D} = \epsilon\mathbf{E}$, where ϵ is the dielectric constant. When we substitute this in Gauss's Law we find that: $\nabla\cdot\mathbf{E} = \dfrac{Q}{\epsilon}$. From Maxwell's equation $\nabla\times\mathbf{E} = 0$ together with the vector identity $\nabla\times\nabla V = 0$, for an arbitrary scalar V, we derive that $\mathbf{E} = -\nabla\psi$, with ψ the potential. From the two derived equations in this paragraph we can derive the Poisson equation [9] $\nabla\cdot\nabla\psi = \nabla^2\psi = -\dfrac{Q}{\epsilon}$. When we write the potential ψ and the charge Q as explicit functions of position we get the Poisson equation.

$$\nabla^2\psi(\mathbf{r}) = -Q(\mathbf{r})/\epsilon. \tag{2.8}$$

Here $Q(\mathbf{r}) = e\sigma(\mathbf{r})\delta(|r| - R) + e\sum_i z_i\rho_i(\mathbf{r})$, where e is the elementary charge, z_i and ρ_i are the valency and density of particles of specie i and $e\sigma$ is the surface charge of the nanotube. The total charge density $Q(\mathbf{r})$, is the external surface charge density plus the total ionic charge density.
Furthermore the boundary condition for ψ can be derived from Gauss's Law in integral form,

$$\oint \mathbf{E}\cdot\mathbf{dA} = \frac{Q_{ext}(\mathbf{r})}{\epsilon} \tag{2.9}$$

$$-\oint \nabla\psi(\mathbf{r})\cdot\mathbf{n}\ d\mathbf{r} = \oint \frac{e\sigma(\mathbf{r})}{\epsilon}. \tag{2.10}$$

The boundary condition for the potential then becomes:

$$\mathbf{n}\cdot\nabla\psi(\mathbf{r}) = -e\sigma(\mathbf{r})/\epsilon \tag{2.11}$$

In this equation $\mathbf{n}$ is the normal to the surface and $e\sigma(\mathbf{r})$ is the surface charge density.

2.4.2 Continuity and particle flux

The continuity equation (F.8) derived in App. F.1 is applicable to all the ion species that move through the fluid. Now we explicitly define the density $\rho_i(\mathbf{r},t)$ and flux $\mathbf{J}_i(\mathbf{r},t)$ from Eq. (F.8) as a function of position $\mathbf{r}$ and time t, which satisfy

$$\frac{\partial\rho_i(\mathbf{r},t)}{\partial t} + \nabla\cdot\mathbf{J}_i(\mathbf{r},t) = 0, \tag{2.12}$$

where i stands for the ion species(Cl^-, Na^+).
There are three different contributions to the flux[10].
(i) The diffusive flux: $\mathbf{J}_i^{diff} = -D_i\nabla\rho_i$, with D_i the diffusion coefficient of species i. This term is also known as Fick's law. The particles flow from a high density to a low density.
(ii) The conductive flux: $\mathbf{J}_i^{cond} = \rho_i\mathbf{v}_i$, where we define the "drift velocity" $\mathbf{v}_i = z_ie\mathbf{E}/6\pi\eta a_i$ in which $\mathbf{E}$ is the electric field, η the solvent viscosity and a_i is the ionic radius of species i. Due to the fluctuation-dissipation relation($D_i = k_BT/6\pi\eta a_i$)[11], we can write $\mathbf{J}_i^{cond} = (D_i/k_BT)z_ie\rho_i\mathbf{E}$, where k_B is the Boltzmann constant and T the temperature.

(*iii*) The advective flux: $\mathbf{J}_i^{adv} = \rho_i \mathbf{u}$, where $\mathbf{u}(\mathbf{r}, t)$ is the velocity of the fluid flow.
By adding the four contributions and substituting $\beta \equiv 1/k_B T$, the result is

$$\mathbf{J}_i = -D_i(\nabla \rho_i + z_i \rho_i \beta e \nabla \psi) + \rho_i \mathbf{u}. \tag{2.13}$$

This equation for the flux is useful to determine the number of particles that move through the nanotube. Equations (2.6), (2.8), (2.12) and (2.13) form the Poisson-Nernst-Planck-Stokes (PNPS) equations.
A dimensionless number that characterises the relative importnace of the the advective flux and the diffusive flux is the Péclet number $\mathrm{Pe} = \frac{\text{advective flux}}{\text{diffusive flux}} = \frac{\mathrm{LU}}{D}$[12], where L and U are typical length and velocity scales respectively. For $\mathrm{Pe} \ll 1$ we can neglect the advective flux and the Equation of the fluxes (2.13) reduces to

$$\mathbf{J}_i = -D_i(\nabla \rho_i + z_i \rho_i \beta e \nabla \psi). \tag{2.14}$$

This simpler equation will be used as an approximation for systems where the fluid velocity is relatively low (for example systems where a low voltage drop is applied as a driving force).

2.4.3 Poisson-Boltzmann distribution

From the flux equation (2.13), we can derive the Poisson-Boltzmann (PB) distribution, an equilibrium distribution of the particle densities weighted by Boltzmann factors. In equilibrium $\mathbf{J}_i = 0$ and $\mathbf{u} = 0$, so that Eq. (2.13) reduces to

$$\nabla \rho_i = -z_i \rho_i \beta e \nabla \psi, \tag{2.15}$$

$$\nabla \ln \rho_i = \frac{\nabla \rho_i}{\rho_i} = -z_i \beta e \nabla \psi, \tag{2.16}$$

$$\rho_i(\mathbf{r}) = \rho_{i,b} \exp[-\beta z_i e \psi(\mathbf{r})]. \tag{2.17}$$

Here $\rho_{i,b}$ is the bulk density of species i, i.e. the density at a position where $\mathbf{u}_i = 0$ and $\psi = 0$. Equation (2.17) is the Poisson-Boltzmann distribution and can be used to compare the particle distributions in the system with their equilibrium distributions.

2.5 Electric double layer

In the inside of the nanotube we consider a solvent near a charged surface. How this surface charge is generated will be explained in Sec. 2.6. The charged surface of the tube attracts counter-ions by Coulomb attraction. This produces a layer of counter-ions screening the surface, this layer of counter-ions together with the surface charge is called the Electric Double Layer (EDL). When we view the EDL as a single layer of counter-ions, this layer is called the Helmholtz Layer, this is seen in Fig. 5(a). If we also consider the thermal fluctuations of the ions we get a diffuse layer of counter-ions screening the surface, this model is called the Gouy-Chapman model and is shown in Fig. 5(b). In reality there are both a sort of Helmholtz layer (now called the Stern layer) and a diffuse layer, this model is shown in Fig. 5(c). In our calculations we use the Gouy-Chapman model, because this simplifies the relevant equations, this is an accurate approximation.
For the EDL these quantities are of interest:

- Zeta potential, ζ. This is the potential at the inner surface, in Fig. 5 it is drawn as Ψ_0.
- Bjerrum length, $\lambda_B = \dfrac{e^2}{4\pi\epsilon k_B T}$.
  The Bjerrum length is a property of the solvent and is equal to the length where the Coulomb interaction potential between two charges e equals $k_B T$. The Bjerrum length indicates the strength of the Coulomb interaction and equals 0.72 nm for water (ϵ_w=78.3) at room temperature.
- Debye length, $\kappa^{-1} = \dfrac{1}{\sqrt{4\pi\lambda_B \rho_s}}$.
  The Debye length is the length over which charge imbalances exist, in the 1-10 nm regime for $\rho_s \approx 1 - 100$ mM in water.

Here ϵ is the permittivity of the solvent and $2\rho_s$ the bulk concentration of the solvent far away from the surface. These quantities together with the Poisson-Boltzmann theory described in Sec. 2.4.3 are relevant to calculate and describe the ion distributions.

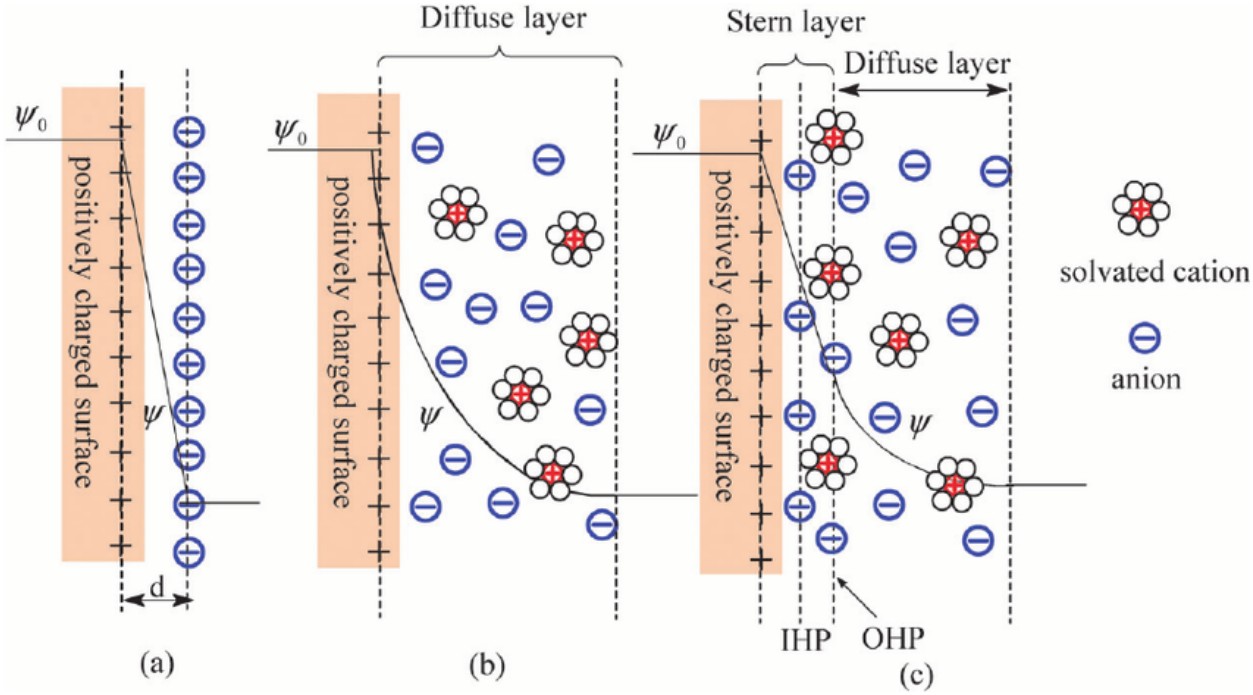

Figure 5: (a) The Helmholtz layer, where the charged surface is completely screened by a single charged layer of counter-ions. (b) The Diffuse layer of the Gouy-Chapman Model, in the Gouy-Chapman model the counter-ions that screen the charged surface are spread out within a diffuse layer. The fact that the counter-ions separate from the surface is due to thermal fluctuations. (c) This modern way of describing the EDL, uses an empirically improvement (this model corresponds better with experimental results) of the Gouy-Chapman model with the Stern layer. This model has a stern layer with fixed counter-ions at the surface. After the Stern layer the diffuse layer begins. IHP refers to the Inner Helmholtz Plane, this is the plane of closest approach to the surface and OHP refers to the Outer Helmholtz Plane, this is where the Stern layer ends and the Diffuse layer begins. Note that in this figure the surface is positively charged while a Boron-Nitride NanoTube(BNNT) is negatively charged and therefore the counter-ions that screen the surface are positive for a BNNT.

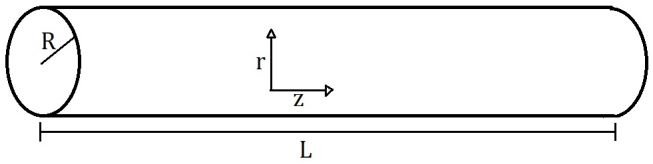

Figure 6: Schematic overview of the nanotube, this tube has a length(L) of 400 nm and a radius(R) of 40 nm. The coordinate axes indicate the radial(r) and axial(z) direction.

2.6 Surface charge and charge regulation

In this section the charged surface of the nanotube will be discussed. In Fig. 6 the tube is shown and the directions of the axes are given. The tube is made of Boron-Nitride which has some interesting physical properties. The Boron-Nitride surface has a hexagonal structure and a hardness comparable to graphite[13]. Furthermore the ionic structure of h-BN (h stand for hexagonal) decreases the electrical conductivity through the material. The surface charge of h-BN becomes very high, 1 C/m^2, for high pH[2]. In most models the surface charge is taken to be homogeneously or the surface is described with a constant potential. However in this section and the rest of this thesis we will use a regulated charge distribution, because this gives a better representation of reality. This charge regulation comes from the fact that flow induces the concentrations of the ion-species to vary along the tube. Surface charge is produced by chemical reactions of the ion species. Therefore the surface charge varies over the tube. First we need to consider how the surface charge is generated, this is roughly speaking possible by four different reactions which can take place at the surface. These reactions involve adsorption and desorption of cat- or anions (positively charged or negatively charged ions, respectively). Here we discuss the desorption of an anion, namely the H^+−ion, because this is the most common reaction in a Boron-Nitride nanotube [2].

$$BN_3 + H_2O \leftrightarrows BN_3\text{-}OH^- + H^+ \text{ with } K = \frac{[BN_3\text{-}OH^-][H^+]}{[BN_3]}. \tag{2.18}$$

All reactions take place at discrete surface sites, the number of chargeable sites is: $[BN_3]+[BN_3 - OH^-] = m(z)$. Furthermore $[H^+] = \rho_{H^+}$, the surface charge density $\sigma = [BN_3 - OH^-]$ and we assume that $m(z) = m$ due to translational invariance. Hence the expression for K becomes $K = \frac{\sigma\rho_{H^+}(z)}{m-\sigma}$, where ρ_{H^+} is now only dependent of the z-coordinate due to the fact that the surface is axially symmetric and has a well defined radius. Therefore the surface charge density takes the form

$$\sigma(z) = \frac{m}{1 + \frac{\rho_{H^+}(z,r=R)}{K}}. \tag{2.19}$$

This equation is used as a boundary condition in our numerical calculations for the surface charge. The value of K is given to be $10^{-5.5}$ mM and $m = 18$ nm^{-2} for a BNNT surface [2]. Note that since we introduced the regulated surface charge we now have another ion specie(H^+) which needs to be considered in our calculations.

2.6.1 Conductivity

The conductivity G, not to be confused with the Gibbs free energy, is a measure in how well a wire or in our case the nanotube conducts a current. We consider a system where a concentration gradient is the driving force for the current. In the linear response regime the current is linearly dependent of the concentration drop, $I \propto \Delta\rho$, for $\Delta\psi = 0$ and $\Delta p = 0$. This relation can also be written as, $I_i = G_i\nabla\mu_i$, where μ_i is the chemical potential for specie i, $\mu_i = k_BT\log(\rho_i)$. Combining those two equations gives

$$I = Gk_BT\nabla\log(\rho) = Gk_BT\frac{\nabla\rho}{\rho}. \tag{2.20}$$

We can write G as a sum of the conductivity of the surface plus the conductivity of the bulk, $G = G_b + G_s$, where G_b is the bulk conductivity and G_s is the surface conductivity. These contributions to the conductivity are inversely proportional to the length of the tube, a longer length means more resistance and thus a smaller current. There is also a dependence on the radius of the tube, when the radius is very small, there will be less ions able to move through the tube. The bulk conductivity will be proportional to the cross-cut of

the tube and the surface conductivity will be proportional to the circumference. Therefore we expect that $G_b = \frac{\pi R^2}{L} g_b$ and $G_s = \frac{2\pi R}{L} g_s$, where g_b and g_s are the bulk and surface conductivity constant respectively. We can rewrite this as

$$G = \frac{\pi R^2 g_b + 2\pi R g_s}{L}. \tag{2.21}$$

Our goal is to find the conductivity constants for the nanotube, so that we can answer our research question. The conductivity constants are a measure of how the conductivity is affected by the radius. However therefore we first need to calculate G for a single system.

3 Measurement method

In this section we describe how the measurements of our research are done. The research was not done experimentally, it was however done by calculations in COMSOL (`https://www.comsol.com`). The geometry in which the physical background is explained is shown in Sec. 2.2. COMSOL uses the Finite-Element Method to calculate several quantities, the fluid velocity, the pressure, the electric potential and the densities of all ion species.
COMSOL has a large number of physical modules, these modules consists of bulk equations and boundary conditions (b.c.'s). In this thesis we use three modules: Electrostatics, Transport of Diluted Species and Creeping Flow. These modules are applied on the geometry shown in Fig. 7, where the nanotube connects two infinite reservoirs.

- Electrostatics,
  On the complete volume of the nanotube we define a charge conservation module and a charge density of $N_A \cdot e \cdot (\rho_{\mathrm{H}^+} + \rho_{\mathrm{Na}^+} - \rho_{\mathrm{Cl}^-})$, where N_A is the Avogadro constant and ρ_i are the ion densities in $\mathrm{mol/m^3}$, note that the units of ρ_i are changed from $1/\mathrm{m^3}$ to $\mathrm{mol/m^3}$. Also we define a relative permittivity of water ϵ_w, where $\epsilon = \epsilon_w \epsilon_0$ in which ϵ_0 is the dielectric constant. On the boundaries we define a grounding potential $\psi = 0$ on the far edges of the baths, a zero charge b.c. ($\mathbf{n} \cdot \mathbf{E} = 0$) on the edge of the bath facing the nanotube and on the tube itself we use the charge regulation model described in Sec. 2.6, $\sigma(z) = \frac{m}{1 + \frac{\rho_{\mathrm{H}^+}(z, r=R)}{K}}$.

- Transport of Diluted Species,
  On the volume we define the diffusion constant of each specie D_i and the fixed and homogeneous temperature T. On the boundaries of the baths we define a concentration $C_{max} = \rho_{\mathrm{Na}^+,u} = \rho_{\mathrm{Cl}^-,u}$ in the upper bath and a concentration $C_{min} = \rho_{\mathrm{Na}^+,d} = \rho_{\mathrm{Cl}^-,d}$ on the lower bath, where u and d refer to up and down, respectively. The boundary condition for the concentration ρ_{H^+} is applied on the upper bath as well as on the lower bath and is taken as $\rho_{\mathrm{H}^+} = 10^{-\mathrm{pH}}$. Also a no-flux b.c. ($\mathbf{n} \cdot \mathbf{J}_i = 0$) is applied to the tube and edges of the baths facing the nanotube. Note that there will be a definite flux through the boundaries of the reservoirs.

- Creeping Flow,
  On the volume we defined the viscosity η and the mass density of water ρ_w, we chose to neglect the inertia term in the Navier-Stokes equation and defined a volume force on the charged particles $\mathbf{f}$. On the boundaries we applied a no-slip b.c. ($\mathbf{u}(R) = 0$). Only on the far edges of the baths have a no-stress b.c. ($[p\mathbb{1} + \eta(\nabla\mathbf{u} + (\nabla\mathbf{u})^T)] \cdot \mathbf{n} = 0$) to be able to have a fluid flow which is not affected by these boundaries.

The standard values of the defined input parameters are given in Table 3. To have a clear view which boundary conditions are applied where, we made a schematic overview in Fig. 7.
The equations that are applied on the volume are shown in Equations (3.1) to (3.4).

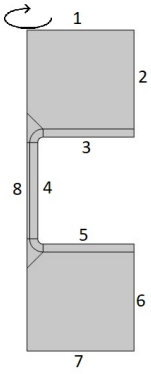

Figure 7: Axis-symmetric representation of a nanotube separating two reservoirs. All boundaries are numbered and their boundary conditions (b.c.'s) are given in this caption.
The Electrostatics b.c.'s are: $\psi = 0$ for (1,2,6,7), zero charge for (3,5) and charge regulation (Sec. 2.6) for (4).
The Transport of Diluted Species b.c.'s are: concentration C_{max} for (1,2), concentration C_{min} for (6,7) and no-flux for (3-5).
The Creeping Flow b.c.'s are: no-slip for (3-5) and no-stress for (1,2,6,7).

$$\eta\nabla^2\mathbf{u} = \nabla p - (e\sigma(\mathbf{r}) + e\sum_i z_i\rho_i(\mathbf{r}))\nabla\psi; \qquad \nabla\cdot\mathbf{u} = 0, \tag{3.1}$$

$$0 = \frac{\partial\rho_i(\mathbf{r},t)}{\partial t} + \nabla\cdot\mathbf{J}_i(\mathbf{r},t), \tag{3.2}$$

$$\mathbf{J}_i = -D_i(\nabla\rho_i + z_i\rho_i\beta e\nabla\psi) + \rho_i\mathbf{u}, \tag{3.3}$$

$$\nabla^2\psi(\mathbf{r}) = -e\sum_i z_i\rho_i(\mathbf{r})/(\epsilon_w\epsilon_0); \qquad \nabla\psi\cdot\hat{\mathbf{n}} = -\frac{e\sigma}{\epsilon_w\epsilon_0}. \tag{3.4}$$

These equations are evaluated in predefined points, e.g. the mesh-points. We used a specific type of meshing for our geometry, the mesh we used for determining the conductivity is shown in Fig. 8. The data from all these mesh-points is processed in Mathematica and thereafter presented in the following section.

4 Results

4.1 Concentration gradient and diffusio-osmotic current

In this section we report the results from the simulations where we applied a concentration gradient over the nanotube. At first we consider the cylinder described in Sec. 2.2. We apply a concentration drop between the two baths and vary the surface charge of the tube, then we measure the electric current through the tube. The so called diffusio-osmotic current from Ref. [2] is written as

$$I_{\mathrm{DO}} = \frac{2\pi R\sigma}{L}\frac{k_BT}{\eta\lambda_B}\Delta\log(\rho_s), \text{ where } \Delta\log(\rho_s) = \log(\frac{C_{max}}{C_{min}}). \tag{4.1}$$

Parameter	Value and unit
ϵ_w	78.3
T	283 K
D^+_{H}	$8.17\cdot10^{-9}$ m^2/s
D^+_{Na}	$1.13\cdot10^{-9}$ m^2/s
D^-_{Cl}	$1.71\cdot10^{-9}$ m^2 s^{-1}
η	$9.54\cdot10^{-4}$ kg m^{-1} s^{-1}
ρ_w	$9.98\cdot10^{2}$ kg m^{-3}
C_{min}	1 mol m^{-3}
m	18 nm^{-2}
K	$10^{-5.5}$ mol m^{-3}

Table 3: The standard parameter values for the nanotube in COMSOL.

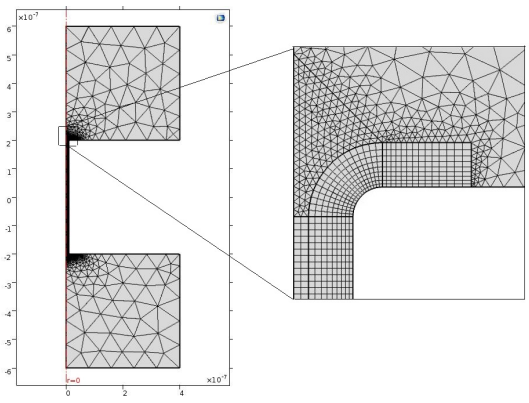

Figure 8: In this figure we show the mesh we use in our study. The part where we zoomed in has a different meshing from the rest of the geometry. This was made in such a way that the high electric forces, which are perpendicular to the charged surface, on the fluid are relatively easily cancelled by the pressure gradient. Note that the geometry is radially symmetric and is rotated around the z-axis (red). Therefore the actual geometry is a 3D system.

The derivation of this equation is given in the supplementary information of Ref. [2].
When we first tried to reproduce the results given in Ref. [2] we encountered large numerical errors. They were caused by spurious flows, these flows are induced by the large volume forces in equilibrium, stemming from the huge osmotic pressure differences that were not compensated by th ehydrostatic pressure.

4.1.1 Reducing spurious flow in equilibrium

To reduce this spurious flow we need to consider the forces acting on the fluid in equilibrium. The Stokes equation (2.6) reduces in equilibrium to,

$$\nabla p = -\mathbf{f} = \epsilon_0 \epsilon_r (\nabla^2 \psi) \nabla \psi = \sum_i z_i e \rho_i \nabla \psi; \qquad \nabla \cdot \mathbf{u} = 0, \tag{4.2}$$

because $\mathbf{u} = 0$ in equilibrium, therefore the pressure gradient needs to cancel the electric force due to the ions in the EDL. In the EDL this electric force is so large that small numerical errors can lead to large spurious flows. The velocity $\mathbf{u}$ and the pressure p are unknowns, p needs to be chosen in such a way that the solution for the velocity field $\mathbf{u}$ also fulfils the incompressibility constraint. For appropriately chosen boundary conditions, the solutions for $\mathbf{u}$ and p are unique (apart from a constant offset of p). Therefore any gradient field $\nabla\omega$ to the force density can be added[14].

$$\nabla (p' - \omega) = \sum_i z_i e \rho_i \nabla \psi; \qquad \nabla \cdot \mathbf{u} = 0, \tag{4.3}$$

We want to reduce the pressure gradient, therefore we need to find a gradient field that exactly cancels the electric force. To find $\nabla\omega$ we consider the flux equation (2.13), which in equilibrium reduces to

$$k_b T \nabla \rho_i = -z_i \rho_i e \nabla \psi. \tag{4.4}$$

Due to the fact that in equilibrium $\mathbf{u} = 0$ and $\mathbf{J}_i = 0$. When we use $\omega = \sum_i k_b T \rho_i$ the Stokes equation reduces to $\nabla p = 0$ in equilibrium. Therefore the new volume force density $\mathbf{f}$ becomes

$$\mathbf{f} = -\sum_i (k_b T \nabla \rho_i + z_i \rho_i e \nabla \psi). \tag{4.5}$$

This is the volume force we will use in our calculations.

4.1.2 Results with the adapted volume force

The results of these simulations are given in App. D. Those are not presented in the thesis itself, because we noticed that the fluid velocities were absurdly high for a nanotube (in the order of magnitude of m/s). We expect the fluid velocity to go to zero as we approach the system without surface charge, due to the fact that there will be no driving force for a fluid velocity since $\nabla\psi = 0$, because there is no excess charge.

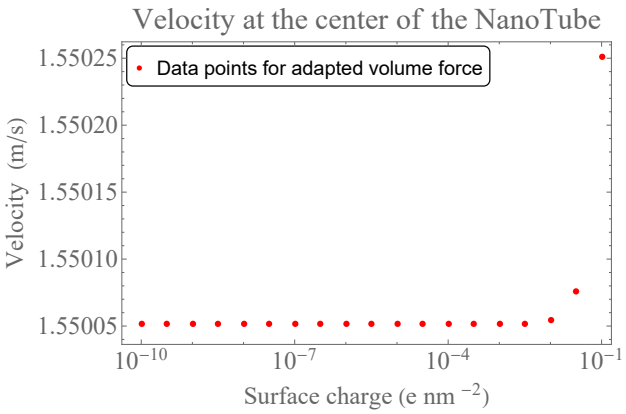

(a) For the adapted volume force to reduce spurious flows. For small surface charge σ there is no velocity dependence.

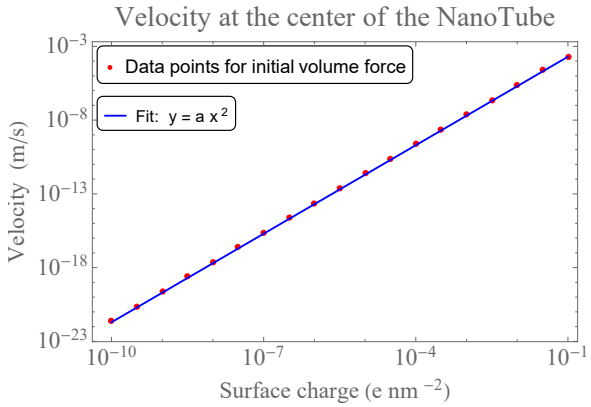

(b) For the initial volume force, with improved mesh to reduce spurious flows. The fit (blue) through the data is in good correspondence with the data.

Figure 9: Surface charge dependence of the axial velocity in a tube of length $L = 1250$ nm and radius $R = 40$ nm, for an applied concentration drop of 0.999 M ($C_{max} = 1$M and $C_{min} = 1$mM), with viscosity $\eta = 9.544 \cdot 10^{-4}$ Pa s. The velocity is measured in the mid-center of the nanotube. Figure (a) and (b) correspond to different volume forces.

When we let the surface charge approach zero, we want to test whether the fluid flow velocity approaches zero as well. In the test we used a concentration drop of 0.999 M in our standard geometry and we varied the surface charge from 10^{-10} to 10^{-1} e nm^{-2}. The result of this test is given in Fig. 9a.
As we can see in Fig. 9a the axial velocity does certainly not approach zero, therefore there must be another driving force, which will probably be the $\nabla\omega$ term which we added to reduce the spurious flow. In conclusion we cannot use the adapted volume force for systems which undergo a concentration drop. This is however the system we wanted to describe, thus we need to work with the initial volume force. To still reduce the spurious flows we need to refine the mesh, so that we have more points where the equations are evaluated. This is done for the results in the following section.

4.1.3 Calculations without spurious flow reducing volume force

The same test was used in the system with the improved mesh and the initial volume force. The result of this test is given in Fig. 9b. As we can see in Fig. 9b the velocity in the center of the tube goes to zero as $v_z \propto \sigma^2$. Therefore the model describes the system well in this scenario. Since the model is now expected to be working according to our expectations we are able to calculate the diffusio-osmotic current as a function of the concentration drop. We investigate the linear response regime, where $I \propto \Delta\rho$. This is the regime in which the variations of the concentration are relatively small. We also did some calculations in the nonlinear regime, those results are given in App. E.
In this linear response regime we can investigate the nanotube as if it were a conducting wire, which has a conductivity that depends on the radius R of the tube, this is done in the following section. However therefore we first need to investigate where the linear response regime breaks down. We used the same settings as in the previous calculation only now we took more datapoints in the range of $\frac{C_{max}}{C_{min}} = [1, 10]$. The results of these calculations are shown in Fig. 10. From Fig. 10 we conclude that the linear response regime breaks down for $\frac{C_{max}}{C_{min}} > 2$, we therefore chose the regime in which $1 \leq \frac{C_{max}}{C_{min}} \geq 1.1$. In this regime we will study the radius dependence of the conductivity.

4.2 Conductivity

The conductivity is calculated for our standard geometry (see Fig. 4), we used a tube with length $L = 400$ nm. We varied the concentration drop from 0 to 0.1 mM, with a bulk concentration(C_{min}) of 1 mM. The nanotube is charged with the charge regulation model described in Sec. 2.6, with $m = 18$ nm^{-2} and pH = 5.5.

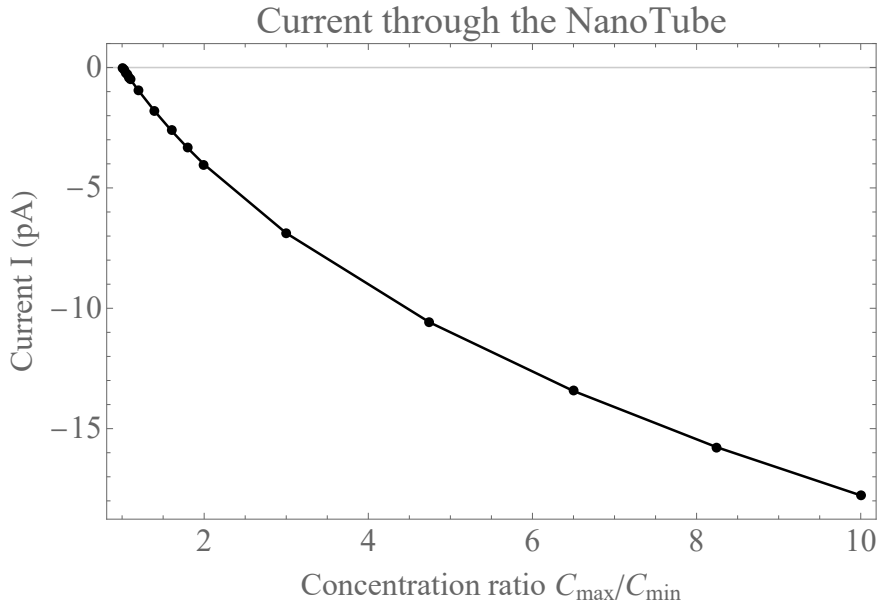

Figure 10: Total current as a result of a concentration drop in a tube of length $L = 1250$ nm and radius of $R = 40$ nm, with viscosity $\eta = 9.544 \cdot 10^{-4}$ Pa s. With diffusion coefficients $D_{\mathrm{Na}} = 1.1 \cdot 10^{-9}$, $D_{\mathrm{Cl}} = 1.7 \cdot 10^{-9}$ and $D_{\mathrm{H}} = 8.2 \cdot 10^{-9}$ all in m^2/s. For a regulated surface charge as in Eq. 2.19 for $m = 18$ nm^{-2}. As concluded from the figure the linear response regime seems to break down for $\frac{C_{max}}{C_{min}} > 2$.

From Fig. 11 we can determine the conductivity, by multiplying the slope with a factor $\frac{L}{k_B T}$ (see Eq. (2.20)). We did this for all calculated data points (For $R = 1-15, 20, 30, 40, 60, 80, 150$ nm). After determining $G(R)$, we can show this result and derive the conductivity constants for this system.
To extract the conductivity constants (from Eq. (2.21)) from our data we can fit three formulas to the data. (*i*) To the unmodified data, where G is a function of R we can use the fit $y = C_1 x^2 + C_2 x$, because this has the same form as Eq. (2.21).
(*ii*) We can also modify our data by multiplying G with a factor $\frac{L}{\pi R}$, Eq. (2.21) then takes the form $G^* \equiv \frac{LG}{\pi R} = R g_b + 2 g_s$, therefore the fit we can use is $y = C_1 x + C_2$.
(*iii*) Another way to modify our data is by multiplying G with a factor $\frac{L}{\pi R^2}$, Eq. (2.21) then takes the form $G^{**} \equiv \frac{LG}{\pi R} = g_b + 2 g_s \frac{1}{R}$, therefore the fit we can use is $y = C_1 + C_2 \frac{1}{x}$.

In Fig. 12 the results for the unmodified data and fit (*i*) are given. Form this figure we can conclude that the fit is in good correspondence with the data for $R > \kappa^{-1}$, where κ^{-1} is the Debye length discussed in Sec. 2.5. However for $R < \kappa^{-1}$ the data seems to differ from our hypothesis, therefore we now modify our data from G to G^*, this is shown in Fig. 13. From Fig. 13 we conclude that our hypothesis is not in correspondence with the data. Namely the bulk conductivity constant g_b seems to be dependent on the radius. In the regime where $R < \kappa^{-1}$, G increases as R increases, this is due to the fact that the current is principally induced in the EDL($R < \kappa^{-1}$). As R increases, while $R < \kappa^{-1}$ is true, more area becomes available for the ions to move through and therefore the conductivity increases. However in the regime $R > \kappa^{-1}$ the conductivity decreases for increasing R, we think this is accrue from the fact that the ions which now move through the middle of the tube are less affected by the surface charge and therefore the current of the Na^+-ions cancels the current from the Cl^--ions. This effect increases for increasing R. Furthermore we can conclude from Fig. 13 that the modified conductivity G^* is maximal for $R = 13$ nm.
It is clear that we cannot fit the straight line from (*ii*) through Fig. 13, however if we only look at the regime where $R > \kappa^{-1}$ we get the data shown in Fig. 14. For this data it is possible to fit a straight line through the data and therefore determine the conductivity constants. For the fit through (*i*) and (*iii*) we decided to also neglect the data with $R < \kappa^{-1}$. The results for these fits are shown in Figures 15 and 16. In the regime where $R < \kappa^{-1}$ the bulk conductivity constant is not constant enough to approximate the data with a linear expression. From the fits through Figures 14 to 16 we derive the conductivity constant of the bulk and the surface for $R > \kappa^{-1}$, these results are shown in Table 4. The bulk conductivity constant we find for the BNNT in the $R > \kappa^{-1}$ regime $g_b = (-1.84 \pm 0.07) \cdot 10^{10}$ S/m^2 and the surface conductivity $g_s = 2326 \pm 16$ S/m. The standard deviations in the results are both within 5 % of the values and therefore we consider the results as reliable.

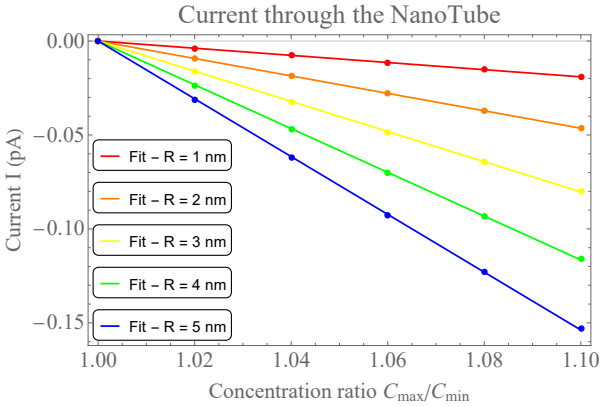

(a) Total current for nanotubes with $R = [1 - 5]$ nm.

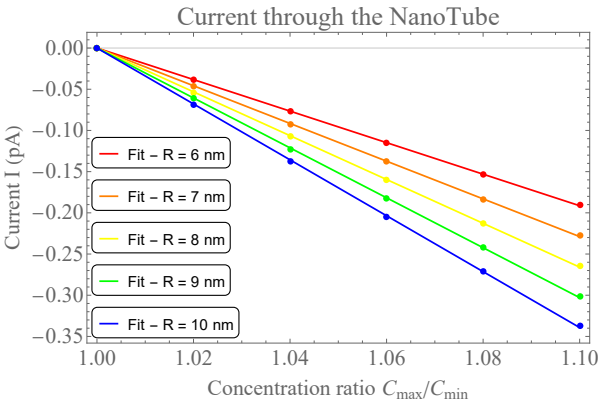

(b) Total current for nanotubes with $R = [6 - 10]$ nm.

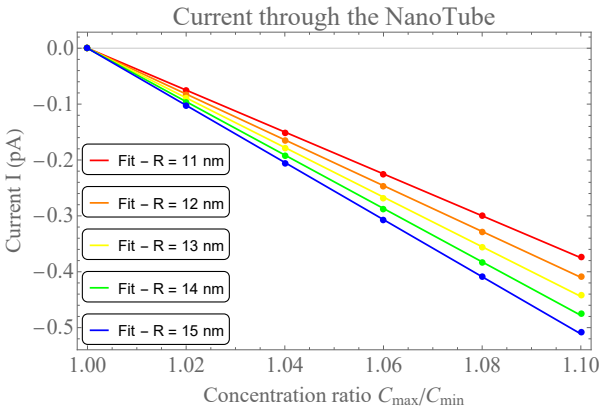

(c) Total current for nanotubes with $R = [11 - 15]$ nm.

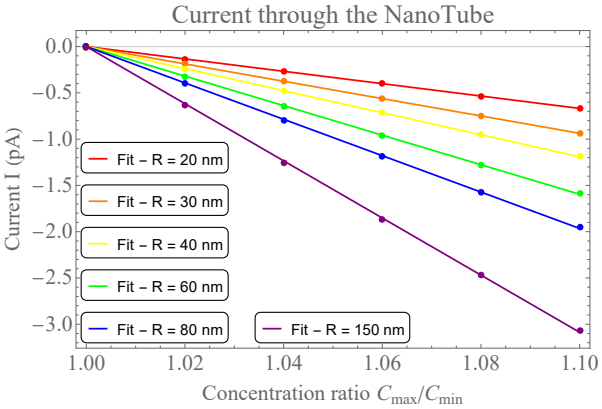

(d) Total current for nanotubes with $R = 20, 30, 40, 60, 80$ and 150 nm.

Figure 11: Total electric current as a result of a concentration drop in a tube of length $L = 400$ nm and a radius $R = [1 - 150]$ nm, with viscosity $\eta = 9.544 \cdot 10^{-4}$ Pa s. With diffusion coefficients $D_{\mathrm{Na}} = 1.1 \cdot 10^{-9}$, $D_{\mathrm{Cl}} = 1.7 \cdot 10^{-9}$ and $D_{\mathrm{H}} = 8.2 \cdot 10^{-9}$ all in m^2/s. For a regulated surface charge as in Eq. (2.19). The conductivity G, which is linearly dependent of the slope, is proportional to the radius and increases as R increases.

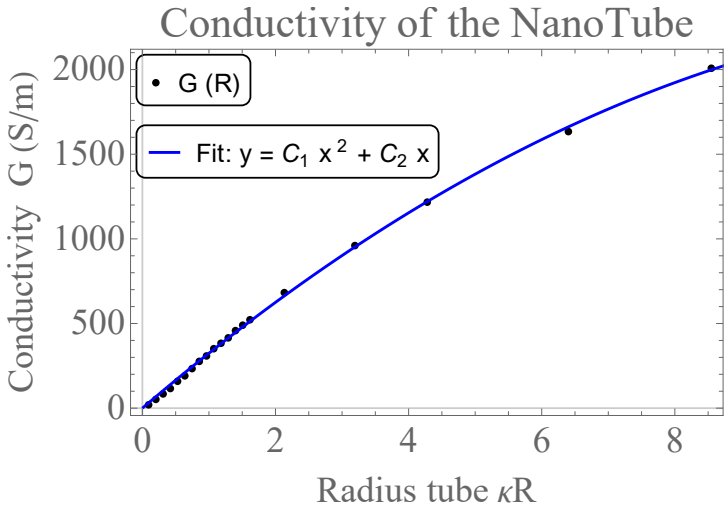

(a) Conductivity (unmodified) as a function of the radius.

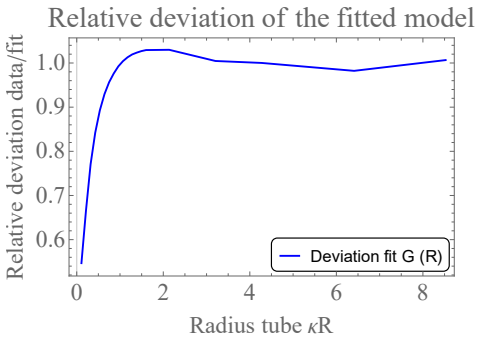

(b) Deviation of the data w.r.t. the fit, this is calculated by dividing the values of the data by the value of the fit. For $\kappa R > 1$ the deviation is small.

Figure 12: Conductivity from a concentration drop in a tube of length $L = 400$ nm and a radius $R = [1-80]$ nm, with viscosity $\eta = 9.544 \cdot 10^{-4}$ Pa s and with diffusion coefficients $D_{\mathrm{Na}} = 1.1 \cdot 10^{-9}$, $D_{\mathrm{Cl}} = 1.7 \cdot 10^{-9}$ and $D_{\mathrm{H}} = 8.2 \cdot 10^{-9}$ all in m^2/s. For a regulated surface charge as in Eq. (2.19).

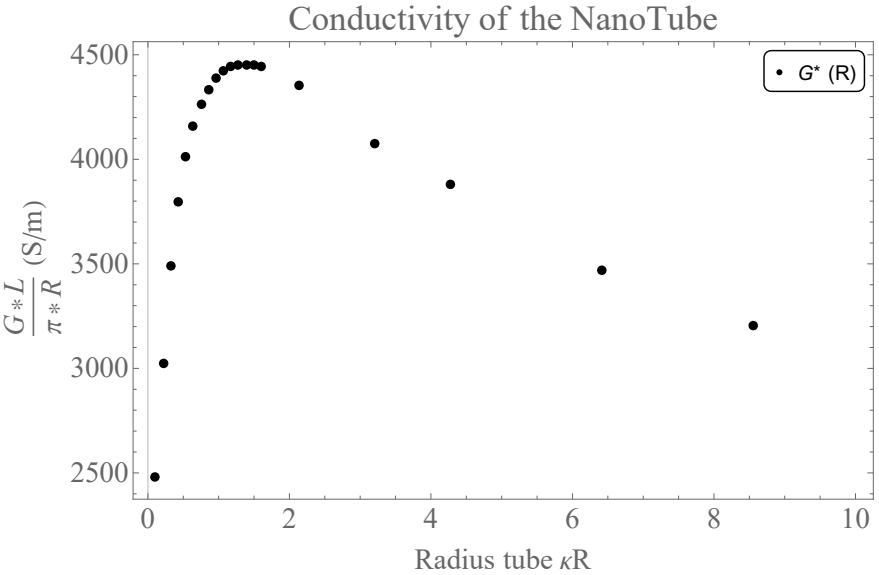

Figure 13: Modified conductivity G^* (G multiplied by a factor $\frac{L}{\pi R}$) from a concentration drop in a tube of length $L = 400$ nm and a radius $R = [1-80]$ nm, with viscosity $\eta = 9.544 \cdot 10^{-4}$ Pa s and with diffusion coefficients $D_{\mathrm{Na}} = 1.1 \cdot 10^{-9}$, $D_{\mathrm{Cl}} = 1.7 \cdot 10^{-9}$ and $D_{\mathrm{H}} = 8.2 \cdot 10^{-9}$ all in m^2/s. For a regulated surface charge as in Eq. (2.19). The modified conductivity is maximal for $R \approx \kappa^{-1}$.

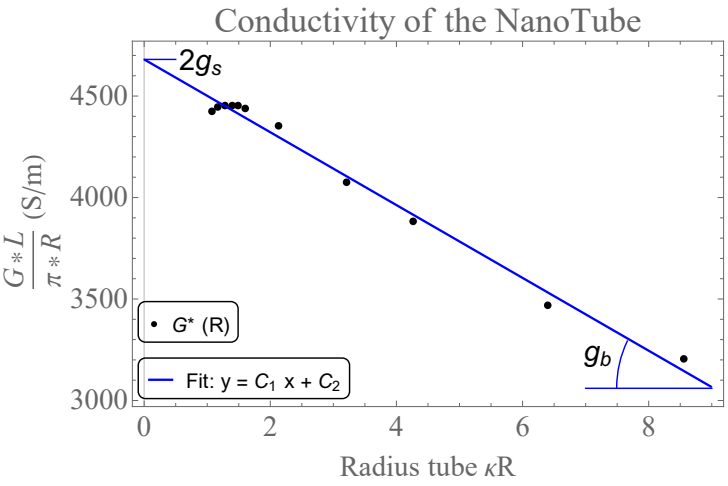

(a) Modified conductivity G^* as a function of the radius.

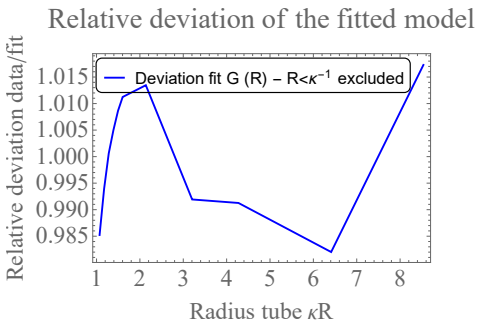

(b) Deviation of the data w.r.t. the fit, this is calculated by dividing the values of the data by the value of the fit. From this figure we conclude that the fit from Fig. 14 (a) is in good correspondence with the data.

Figure 14: Modified conductivity G^* (G multiplied by a factor $\frac{L}{\pi R}$) from a concentration drop in a tube of length $L = 400$ nm and a radius $R = [10 - 80]$ nm, with viscosity $\eta = 9.544 \cdot 10^{-4}$ Pa s and with diffusion coefficients $D_{\text{Na}} = 1.1 \cdot 10^{-9}$, $D_{\text{Cl}} = 1.7 \cdot 10^{-9}$ and $D_{\text{H}} = 8.2 \cdot 10^{-9}$ all in m^2/s. For a regulated surface charge as in Eq. (2.19).

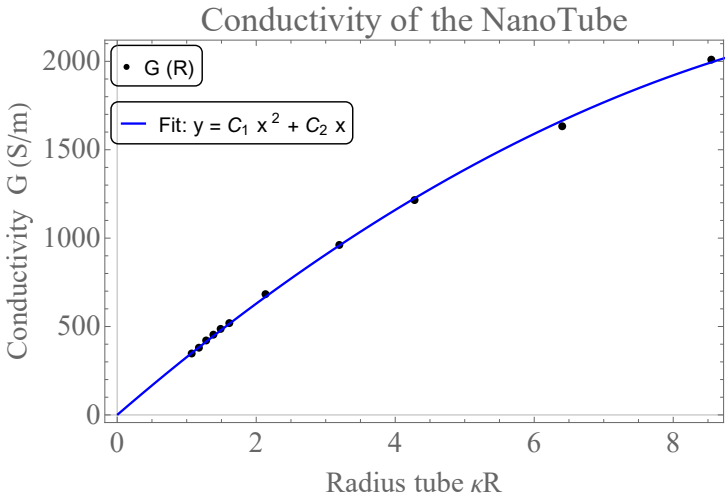

(a) Conductivity (unmodified) as a function of the radius.

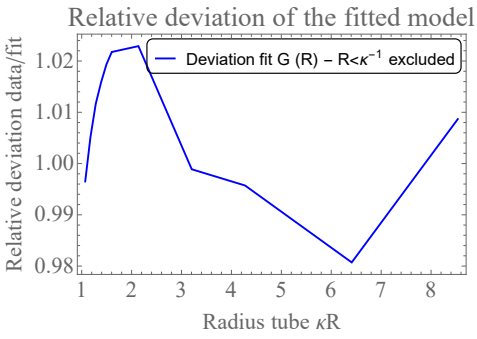

(b) Deviation of the data w.r.t. the fit, this is calculated by dividing the values of the data by the value of the fit. From this figure we conclude that the fit from Fig. 15 (a) is in good correspondence with the data.

Figure 15: Conductivity from a concentration drop in a tube of length $L = 400$ nm and a radius $R = [10-80]$ nm, with viscosity $\eta = 9.544 \cdot 10^{-4}$ Pa s and with diffusion coefficients $D_{\text{Na}} = 1.1 \cdot 10^{-9}$, $D_{\text{Cl}} = 1.7 \cdot 10^{-9}$ and $D_{\text{H}} = 8.2 \cdot 10^{-9}$ all in m^2/s. For a regulated surface charge as in Eq. 2.19.

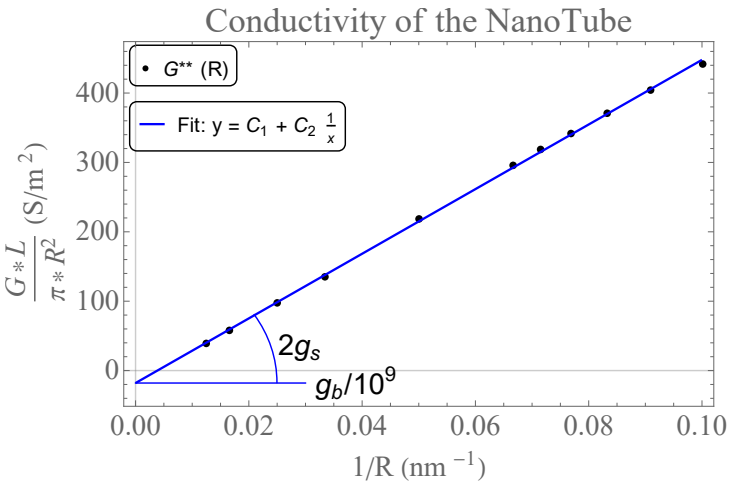

(a) Modified conductivity G^{**} as a function of the radius.

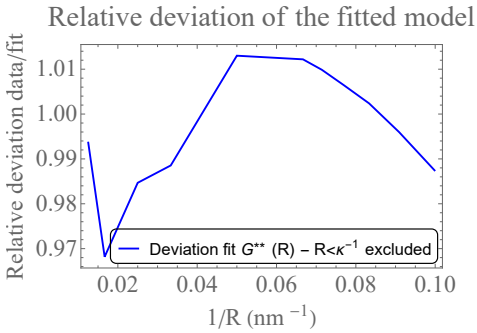

(b) Deviation of the data w.r.t. the fit, this is calculated by dividing the values of the data by the value of the fit. From this figure we conclude that the fit from Fig. 16 (a) is in good correspondence with the data.

Figure 16: Modified conductivity G^{**} (G multiplied by a factor $\frac{L}{\pi R^2}$) from a concentration drop in a tube of length $L = 400$ nm and a radius $R = [10 - 80]$ nm, with viscosity $\eta = 9.544 \cdot 10^{-4}$ Pa s and with diffusion coefficients $D_{\text{Na}} = 1.1 \cdot 10^{-9}$, $D_{\text{Cl}} = 1.7 \cdot 10^{-9}$ and $D_{\text{H}} = 8.2 \cdot 10^{-9}$ all in m^2/s. For a regulated surface charge as in Eq. (2.19).

Fit/constant	g_b (S/m^2)	g_s (S/m^2)
(i)	-1.81·10^{10}	2309
(ii)	-1.92·10^{10}	2340
(iii)	-1.80·10^{10}	2329
Average	(-1.84±0.07)·10^{10}	2326±16

Table 4: Bulk and surface conductivity constants for a tube of length $L = 400$ nm and a radius $R = [10 - 80]$ nm ($R > \kappa^{-1}$), with viscosity $\eta = 9.544 \cdot 10^{-4}$ Pa s and with diffusion coefficients $D_{\text{Na}} = 1.1 \cdot 10^{-9}$, $D_{\text{Cl}} = 1.7 \cdot 10^{-9}$ and $D_{\text{H}} = 8.2 \cdot 10^{-9}$ all in m^2/s. For a regulated surface charge $\sigma(z) = \dfrac{m}{1 + \frac{\rho_{\text{H}^+}(z, r=R)}{K}}$ as derived in Sec. 2.6.

5 Conclusion

In this thesis we studied a Boron-Nitride nanotube with a regulated surface charge and we investigated the conductivity when the nanotube connects two baths with different ion concentrations, e.g. fresh water and sea water. Before focussing on the conductivity of the nanotube we tried to reproduce the results found in Ref. [2]. However, we encountered several problems during the calculations. At first we had to deal with spurious flows, flows induced by numerical errors. To reduce these numerical errors we tried to alter the volume force to get smaller pressure gradients. This worked for systems where there was no concentration gradient, the spurious flows had reduced, when we however turned back to our system with a concentration gradient a large non-physical driving force was found. This caused us to return to our initial volume force, with spurious flows. We had to reduce these spurious flows in another way, to accomplish this we refined the mesh at cost of our calculation time. Now we were ready to reproduce the results from Ref. [2]. When we analysed the data we found that the current was sign-dependent of the concentration ratio, this was very surprising. We chose to study the linear response regime where $I \propto (\frac{C_{max}}{C_{min}} - 1)$, because this was more insightful, the regime where this linear response is broken is an interesting continuation of this research.
For the linear response regime we compared the results for the conductivity to a conducting wire, which has a surface and bulk contribution to the conductivity. We found that in the regime where the radius R is smaller than the Debye length κ^{-1} (so $R < \kappa^{-1}$) the bulk conductivity constant is positive, while in the regime $R > \kappa^{-1}$ the bulk conductivity constant is negative. We were able to find the bulk conductivity

constant and the surface conductivity constant in the $R > \kappa^{-1}$ regime the results of the analysis are given in Table 4. The results of different methods of fitting agree with each other and therefore we consider the results as reliable. Further research is needed to get a better understanding of the phenomenon which induce the diffusio-osmotic current in the high concentration gradient limit. Furthermore we suggest that the conductivity constants can be determined for larger pH values, because in Ref. [2] the diffusio-osmotic current was larger for increasing pH values. This might result in a more efficient way of generating blue energy.

References

[1] Website about the projects on the Afsluitdijk, https://www.deafsluitdijk.nl/projecten/blue-energy/.

[2] A. Siria, P. Poncharal, A.-L. Biance, R. Fulcrand, X. Blase, S. T. Purcell, and L. Bocquet, Nature **494** (2013).

[3] A. G. Dickson and C. G. Macklemore, *Handbook of Methods for the Analysis of the Various Parameters of the Carbon Dioxide System in Sea Water.* (U. S. Department of Energy, 1994), 2nd ed., ORNL/CDIAC-74, URL https://www.nodc.noaa.gov/ocads/oceans/handbook.html.

[4] S. J. Blundell and K. M. Bludell, *Concepts in Thermal Physics* (Oxford University, Oxford, 2010), 2nd ed., ISBN 9780199562107.

[5] J. W. Post, Ph.D. thesis, Wageningen University & Research (2009).

[6] https://www.seatemperature.org/europe/netherlands/.

[7] R. Su, Yale Scientific (2013), http://www.yalescientific.org/2013/02/the-elixir-of-life-generating-electricity-from-water/.

[8] Illinois Institue of Technology, https://web.iit.edu/sites/web/files/departments/academic-affairs/academic-resource-center/pdfs/Navier_Stokes.pdf.

[9] D. J. Griffiths, *Introduction to Electrodynamics* (Prentice-Hall International, New Jersey, 1999), 3rd ed., ISBN 0139199608.

[10] R. van Roij, *Dictate Soft Condensed Matter Theory* (2018).

[11] U. M. B. Marconi, A. Puglisi, L. Rondoni, and A. Vulpiani, physrep **461**, 111 (2008), 0803.0719.

[12] https://en.wikipedia.org/wiki/P%C3%A9clet_number.

[13] G. D., B. Y., T. C.C., and Z. C.Y., Advanced Materials **19**, 2413 (2007), https://onlinelibrary.wiley.com/doi/pdf/10.1002/adma.200700179.

[14] G. Rempfer, G. B. Davies, C. Holm, and J. de Graaf, The Journal of chemical physics **145**, 044901 (2016).

[15] Proceedings of the Royal Society of London A: Mathematical, Physical and Engineering Sciences **133**, 106 (1931), ISSN 0950-1207, http://rspa.royalsocietypublishing.org/content/133/821/106.full.pdf, URL http://rspa.royalsocietypublishing.org/content/133/821/106.

[16] J. Marshall and R. A. Plumb, *Atmosphere, Ocean and Climate Dynamics*, vol. 93 (Elsevier Academic Press, Oxford, 2008), 1st ed., ISBN 9780125586917.

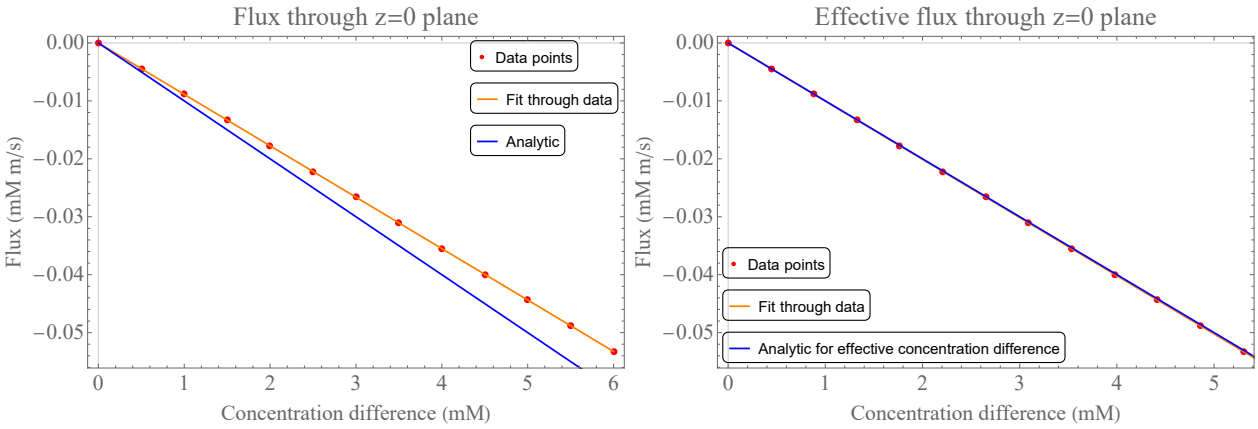

Figure 17: Left: We consider a tube of length $L = 100$ nm and radius $R = 10$ nm connecting two baths with concentration $\rho_1 = [0, 6]$ mM and $\rho_2 = 0$ for bath 1 and bath 2 respectively. In this figure the flux through the middle of the tube is given as a function of concentration difference. The data shows that there is less flux then expected from the analytical expression. This is because the concentration difference already decreased in the baths.
Right: To check whether the deviation from the left figure was accrue from the decrease in concentration difference between the baths. The analytic expression in this part takes the concentration difference between the upper and lower part of the tube. From this figure it is shown that the data perfectly corresponds to what is expected from the analytical expression.

A Basic physics to test model

In this appendix we discuss some basic physical theories which we tested on our model in COMSOL. The results of these calculations are shown in several figures.

A.1 Fick's law

In this section we discuss the transport of diluted species through the cylindrical nanotube, with Length $L = 100$ nm and radius $R = 10$ nm (see Fig. 4). We applied a concentration gradient between the edge(1) of Bath A end edge(3) of Bath C. There was no pressure gradient and there were no electric charges. Therefore Eq. 2.13 reduces to Fick's law: $\mathbf{J} = -D\nabla\rho$. In COMSOL we varied the concentration gradient from 0 to 6 mM and measured the flux through the $z = 0$ plane, which is the plane in the middle of the nanotube. The results of these calculations are shown in Fig. 17. When we calculate an analytical expression $\mathbf{J} = -D\nabla\rho \Rightarrow \mathbf{J} = -D\dfrac{\Delta\rho}{L}$, where we assumed that the concentration only varies in the nanotube with length L. As we can see in the left figure of Fig. 17 the flux that is analytically expected is higher. Therefore we checked what the concentrations were between the upper part of the tube an the lower part. From this we saw that the concentration gradient decreased a little in the baths. Therefore we show in right part of Fig. 17 the analytic expression for the effective concentration difference. Therefore we conclude that the data perfectly corresponds to this analytic expression.

A.2 Poiseuille flow

In this section we discuss the Poiseuille flow through the nanotube. Poiseuille flow is a pressure-induced flow. We discuss the Poiseuille flow for a cylindrical system (the nanotube, again with $L = 100$ and $R = 10$ nm). In this section there will be no diluted species nor charge therefore the Stokes equation 2.6 reduces to $\eta\nabla^2\mathbf{u} = -\nabla p$; $\nabla\cdot\mathbf{u} = 0$. Solving these equations for cylindrical coordinates and no-slip boundary conditions, where the pressure is applied at Bath A (the upper Bath), gives the velocity profile: $v_z(r) = -\dfrac{\partial p}{\partial z}\dfrac{1}{2\eta}r(R-r)$ [10], where $v_z(r)$ is the velocity in the z-direction, r the distance to the z-axis and R the radius of the

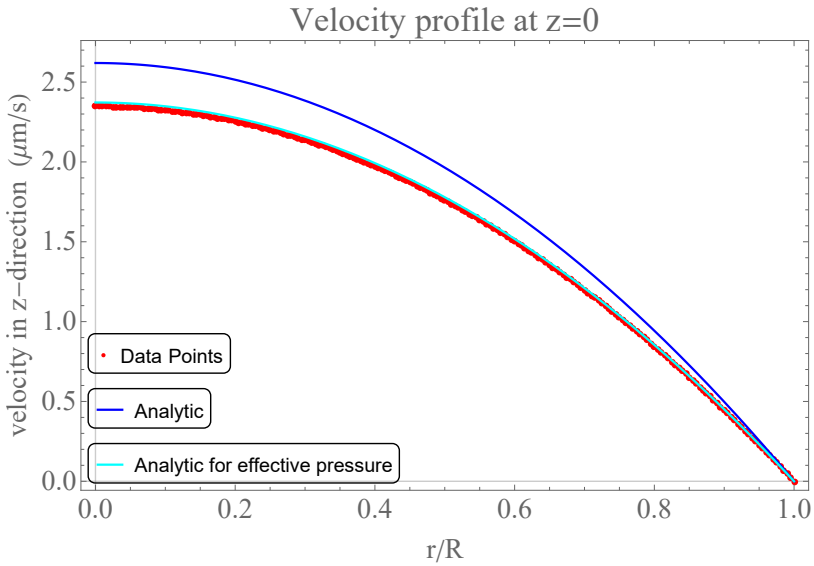

Figure 18: Radial dependence of the axial velocity $v_z(r)$ in a tube of length $L = 100$ nm and radius $R = 10$ nm, for an applied pressure drop of $\Delta p = 10$ Pa, with viscosity $\eta = 9.544 \cdot 10^{-4}$ Pa s. The analytic expression (blue)[10], is valid for the assumption that the pressure only changes inside the tube, while the expression for the effective pressure use the actual pressure drop measured in the tube (cyan). The profile of $v_z(r)$ is seen to be in good correspondence with the expression which uses the effective pressure.

nanotube as we can see in Fig. 4. The results of the calculations together with the analytical expression are shown in Fig. 18.

For the analytic expression we estimated $\frac{\partial p}{\partial z}$ to be constant and equal to $\frac{\Delta p}{L}$. When we improved the analytic expression by measuring the effective pressure difference we used $\frac{\partial p}{\partial z} = \frac{\Delta p_{eff}}{L}$. The results of the comparison of the data with the improved analytic solution are also shown in Fig. 18. We can see that the data is in accordance with the analytical expression.

After recovering the analytical result for the Poiseuille flow we wanted to determine the influence of the length of the tube and the influence of rounding the edges of the nanotube. First we considered the influence of rounded edges, because rounded edges give rise to a more continuous flow which is easier to calculate. We varied the edges from a radius of 1 nm to a radius of 15 nm, the radius of the rounded corner will be called R_c. We used the same settings as in the first calculations of the poiseuille flow and got the results that are shown in Fig. 19.

As we can see in Fig. 19 the radius of the corner gives rise to a relatively small error. We calculated this error to be 5.5 % for $R_c = 5$ nm, with respect to the system where the radius R_c of the curvature of the corner of the tube is 0. This error is 18.6 % for a $R_c = 15$ nm. Because the solution converges easier for $R_c = 5$ nm, we will use this for our standard geometry. Secondly we wanted to investigate the influence of the length of the nanotube. We used the same settings as in the previous calculations of the poiseuille flow only now we took $L = 1000$ nm. Again we varied R_c for this length, the results are shown in Fig. 20.

As we can see in Fig. 20 the radius of the corner gives rise to a very small error with respect to the situation where the corners are not rounded. We calculated this error to be 0.5 % for a R_c of 5 nm and 2.1 % for a R_c of 15 nm. These errors are thus much smaller for a longer tube. Also we conclude from the results that for a long nanotube the effective pressure is as good as equal to the pressure difference that was applied. This we can conclude from the fact that the data is in accordance with the analytical expression in Fig. 20. The observant reader might have noticed that the maximum velocity in Fig. 20 is lower by a factor of 10, this is a result of the fact that the pressure gradient is now spread over a longer distance (a 10 times longer distance).

B Poisson-Boltzmann distributions

B.1 Poisson-Boltzmann for a charged plane

In this section we calculate the potential with Poisson Boltzmann theory. The system we describe is a homogeneously charged surface in the $z = 0$ plane. In the region above the plane ($z > 0$) there is a

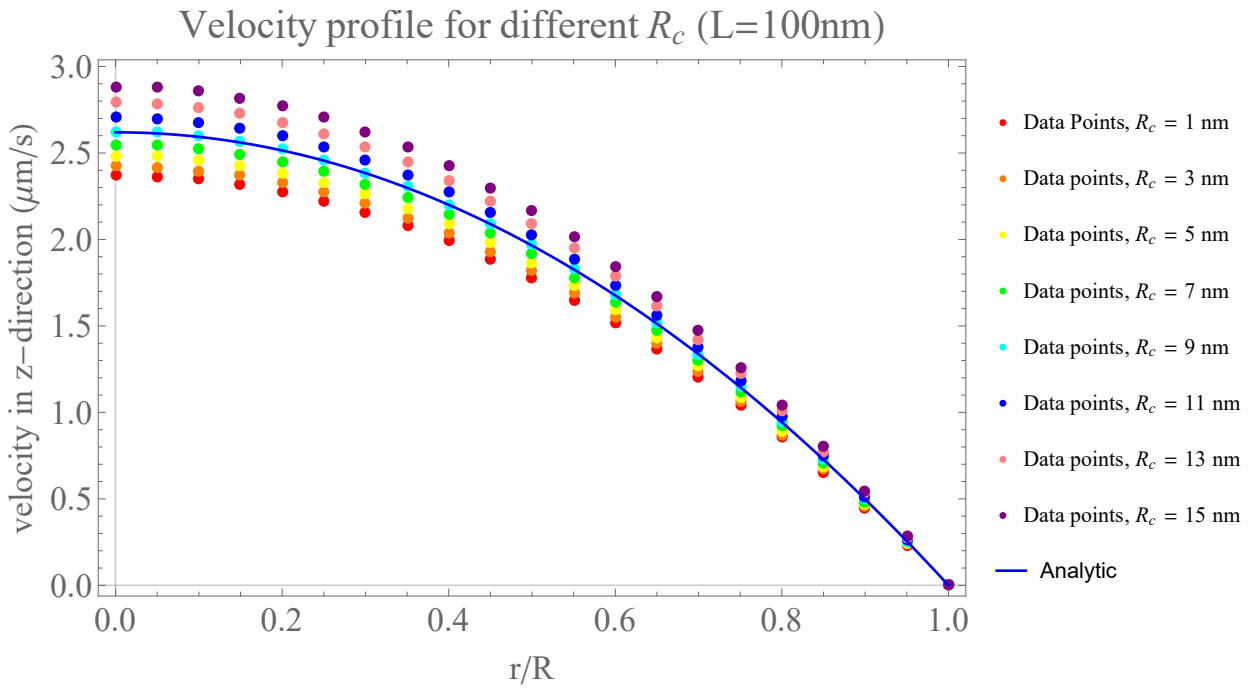

Figure 19: Radial dependence of the axial velocity $v_z(r)$ in a tube of length $L = 100$ nm and radius $R = 10$ nm, for an applied pressure drop of $\Delta p = 10$ Pa, with viscosity $\eta = 9.544 \cdot 10^{-4}$ Pa s. The profile of $v_z(r)$ is seen to be dependent on the radius of the curvature R_c at the corners of the tube.

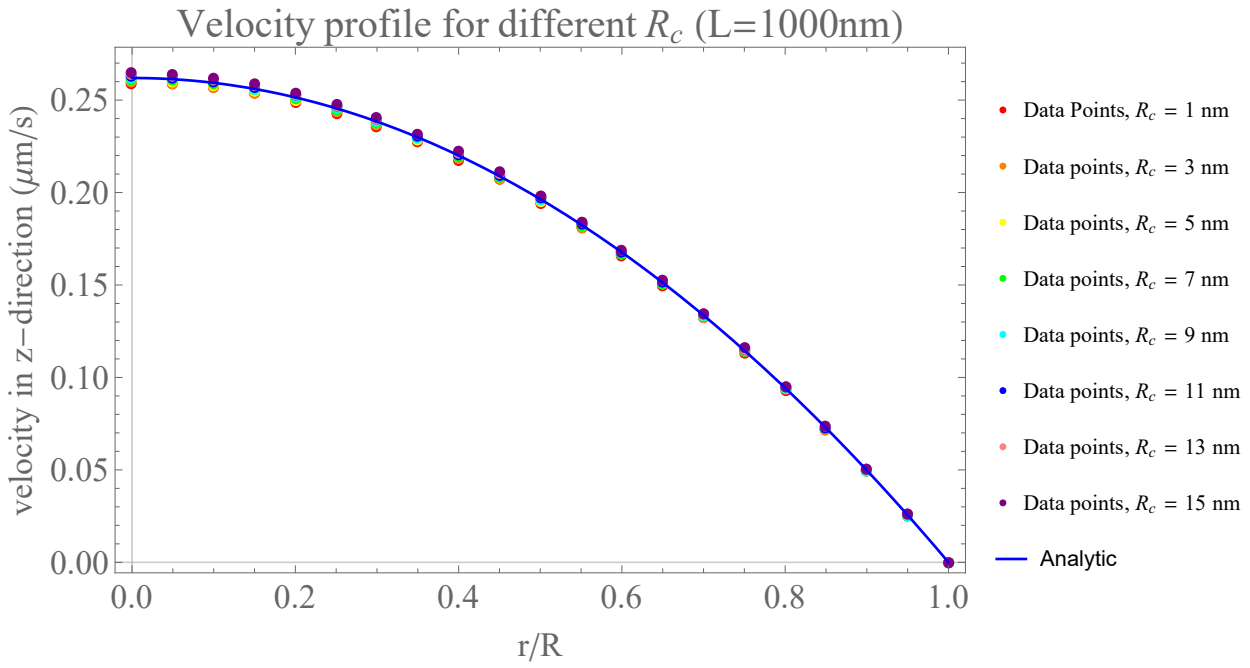

Figure 20: Radial dependence of the axial velocity $v_z(r)$ in a tube of length $L = 1000$ nm and radius $R = 10$ nm, for an applied pressure drop of $\Delta p = 10$ Pa, with viscosity $\eta = 9.544 \cdot 10^{-4}$ Pa s. The profile of $v_z(r)$ is seen to be only weakly dependent on the radius of the curvature R_c at the corners of the tube.

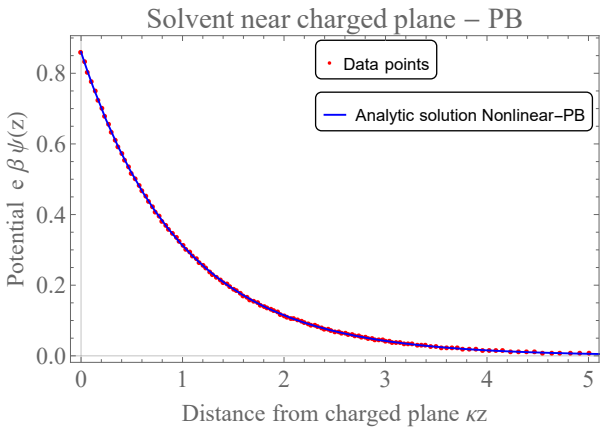

Figure 21: The dimensionless potential $\phi(z)$ as a function of the distance from a charged infinite plane, for a surface charge of $\sigma = 0.01e\text{nm}^{-2}$ and viscosity $\eta = 9.544 \cdot 10^{-4}$ Pa s. As seen in the figure the calculated values almost perfectly match the analytic solution.

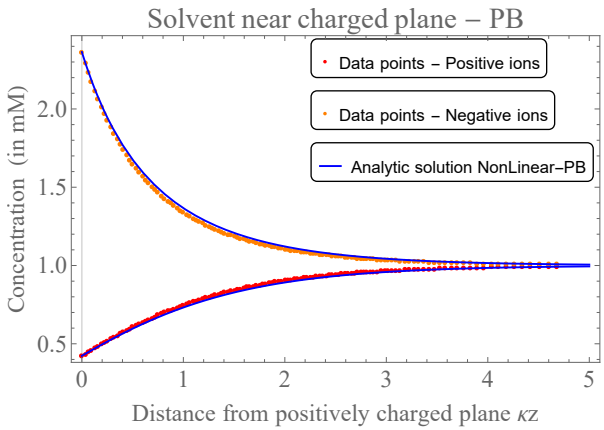

Figure 22: The concentration of the cations (red) and anions (orange) as a function of the distance from the charged infinite plane, for a surface charge of $\sigma = 0.01e\text{nm}^{-2}$ and viscosity $\eta = 9.544 \cdot 10^{-4}$ Pa s. As seen in the figure the calculated values almost perfectly match the analytic solution.

solvent, namely water. The other half space ($z < 0$) is a dielectric. The solution for the potential can be found by solving the Poisson equation 2.8 and using the Poisson-Boltzmann distribution **??**. With some hard mathematics the analytic solution B.1 is found (See the dictate Soft Condensed Matter Theory for a derivation [10]):

$$\phi(z) = 2 \ln \frac{1 + \gamma \exp[-\kappa z]}{1 - \gamma \exp[-\kappa z]}, \tag{B.1}$$

where $\phi(z) = \beta e \psi(z)$ is the dimensionless potential and κ is the inverse Debye length as discussed in Sec. 2.5. $\gamma = \dfrac{\sqrt{1 + (y/2)^2} - 1}{y/2}$, where $y = \dfrac{4\pi\lambda_B\sigma}{\kappa}$, with λ_B the Bjerrum length which was also discussed in Sec.2.5 and σ the surface charge.
The dimensionless potential was calculated for $\sigma = 0.01$ e nm^{-2} and plotted together with the analytic solution B.1, this is shown in Fig. 21. From this result we verified that our data analysis for PB-theory was correctly done due to the fact that the data is in accordance with the analytic solution.

B.2 Poisson-Boltzmann for outside a charged sphere

In this section we calculate the potential with Poisson Boltzmann theory. The system we describe is a homogeneously charged sphere in a solvent (water). The solution for the potential around the charged sphere can be found by solving the Poisson equation 2.8 and using the Poisson-Boltzmann distribution **??**. With some hard mathematics the analytic solution B.2 is found (See the dictate Soft Condensed Matter Theory for a derivation [10])

$$\phi(r) = 4\pi a^2 \sigma \lambda_B \frac{\exp(\kappa a)}{1 + \kappa a} \frac{\exp(-\kappa r)}{r}, \tag{B.2}$$

In which a is the spheres radius, σe is the charge density, λ_B is the Bjerrum length and κ is the Debye length which are discussed in Sec. 2.5.
For a surface charge of $\sigma = 0.0001e$ nm^{-2} we simulated the ion distributions and the potential, these results are shown in Figures 23 and 24. As seen in the figures the calculated values almost perfectly match the analytic solutions.

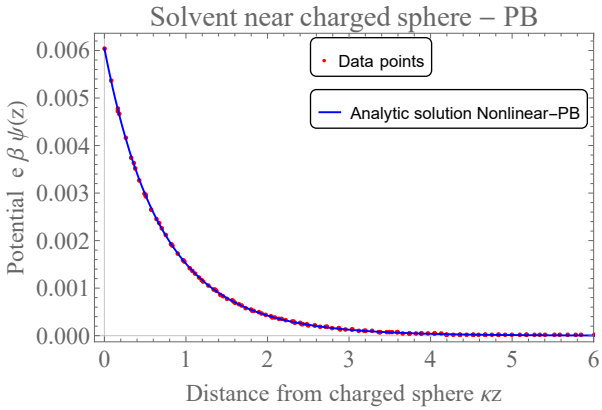

Figure 23: The dimensionless potential $\phi(r)$ as a function of the distance from a charged sphere, for a surface charge of $\sigma = 0.0001e$ nm^{-2} and viscosity $\eta = 9.544 \cdot 10^{-4}$ Pa s. As seen in the figure the calculated values almost perfectly match the analytic solution described in App. B.2.

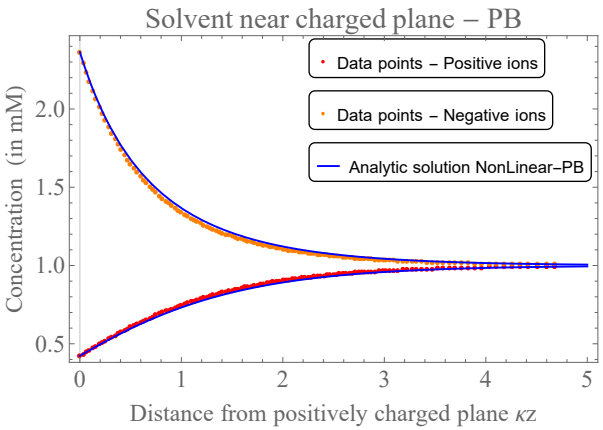

Figure 24: The concentration of the cations (red) and anions (orange) as a function of the distance from the charged sphere, for a surface charge of $\sigma = 0.0001e$ nm^{-2} and viscosity $\eta = 9.544 \cdot 10^{-4}$ Pa s. As seen in the figure the calculated values almost perfectly match the analytic solution, which is described in Sec. 2.4.3.

C Smoluchowski

In this section we consider a positively charged spherical particle in a solvent. We apply an electric field over the solvent, therefore the anions which are attracted to the surface will move against the electric field, this will induce a fluid flow. We calculate the velocity of the particle as a function of the applied voltage drop. We consider a particle with a Radius of 25 nm in a solvent with an ion concentration of 1 mM. The electric field over the solvent comes from the voltage drop over a distance of 1 μm. We take the surface charge to be 0.01 elementary charges per nm squared, because then we are still in the linear PB regime. From the dictate of soft condensed matter [10] we know that $w = -\frac{\epsilon\zeta}{\eta}E$, where ζ is the zeta potential which we defined in Sec. 2.5 and w is the velocity in the z-direction. Due to the fact we are in the linear regime, we can use $\zeta = \frac{Z\lambda_B}{(1+\sqrt{1+\kappa R})R}$ from the same dictate. The results are shown in Fig. 25. As we can see in the figure, the data is in good correspondence with the analytic expression (which makes use of Henry's Function[15]), therefore we can conclude that the physics used to describe this model are sufficient.

D Results with the adapted volume force

We applied a concentration drop of 0.1 mM with a reference density of 0.1 mM over the tube. We used a regulated surface charge with 18 chargeable sites nm^{-2}, the radius and length are 40 nm and 1250 nm respectively. With these conditions we calculated the velocity profile in the middle of the tube, the results are shown in Fig. 26. From this figure we conclude that the velocity profile is the same along the z-direction of the tube, not taking into account the effects at the inlet and outlet of the tube.
The charge density inside the tube and the densities of all individual ion species are shown in Figures 27 to 30. From these figures we can conclude that the surface charge has a large impact on the ion distributions, which also can be derived by considering the PB-distributions for the EDL. Unfortunately we cannot use the results, where we calculated the diffusio-osmotic current due to the fact that the velocity of the fluid was caused by a non-physical driving force.

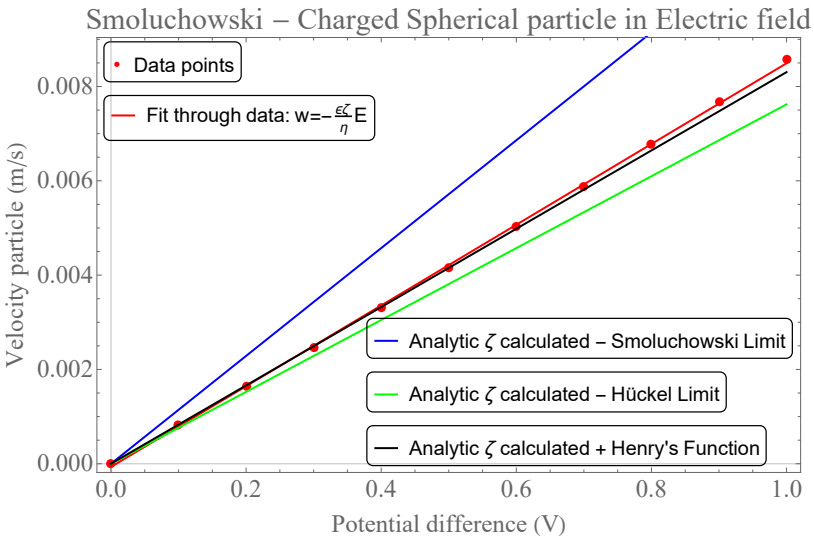

Figure 25: Velocity w of a charged spherical particle of radius $R = 25$ nm and surface charge $\sigma = 0.01e$ nm^{-2} in a solvent in an electric field. The applied voltage drop $V = [0, 1]$ V is applied over a distance $\Delta x = 1$ μm. The concentration of the ions in the solvent $\rho_s = 1$ mM. Therefore $\kappa R = 2.67$. The Hückel-limit is valid for κR $\ll 1$ and the Smoluchowski-limit is valid for κR $\gg 1$. The Henry's Function is used for giving the analytic expression for the interval between the two limits [15]. As seen in the figure the data is in good correspondence with the analytical expression.

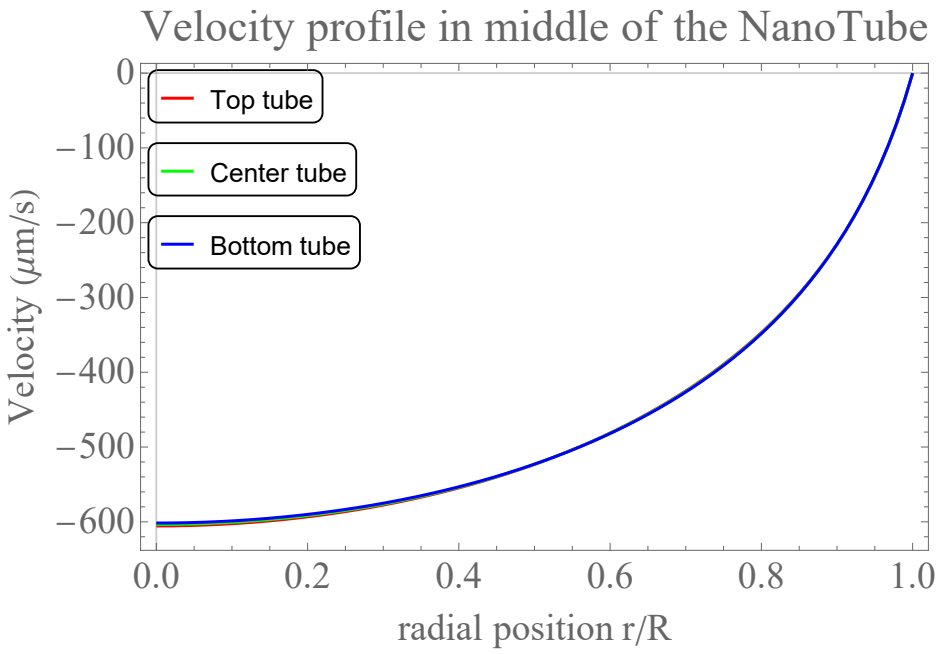

Figure 26: Axial velocity in a tube of length $L = 1250$ m and radius $R = 40$ nm, for an applied concentration drop of 0.1 mM, with viscosity $\eta = 9.544 \cdot 10^{-4}$ Pa s. The velocity is measured in the middle, top and bottom of the nanotube.

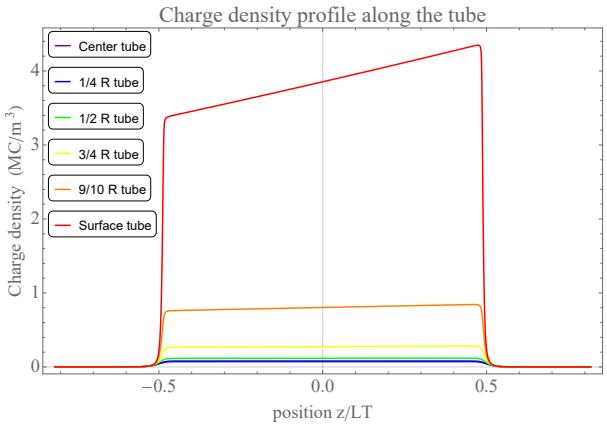

Figure 27: Charge density in a tube of length $L = 1250$ m and radius $R = 40$ nm, for an applied concentration drop of 0.1 mM, with viscosity $\eta = 9.544 \cdot 10^{-4}$ Pa s. The surface is charged according to the charge regulation model described in Sec. 2.6.

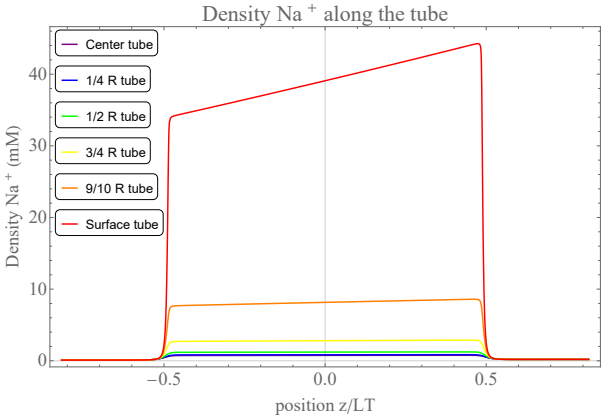

Figure 28: Density of Na^+-ions in a tube of length $L = 1250$ m and radius $R = 40$ nm, for an applied concentration drop of 0.1 mM, with viscosity $\eta = 9.544 \cdot 10^{-4}$ Pa s. The surface is charged according to the charge regulation model described in Sec. 2.6.

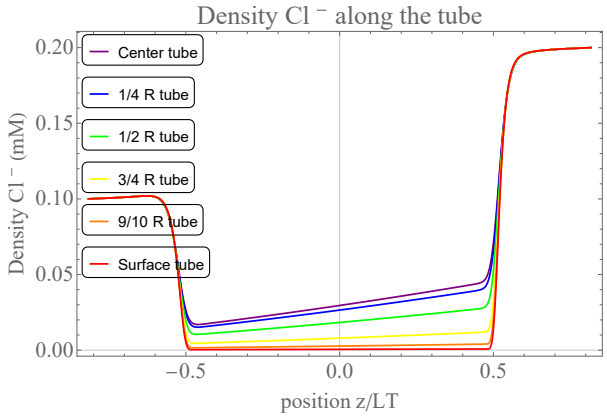

Figure 29: Density of Cl^--ions in a tube of length $L = 1250$ m and radius $R = 40$ nm, for an applied concentration drop of 0.1 mM, with viscosity $\eta = 9.544 \cdot 10^{-4}$ Pa s. The surface is charged according to the charge regulation model described in Sec. 2.6.

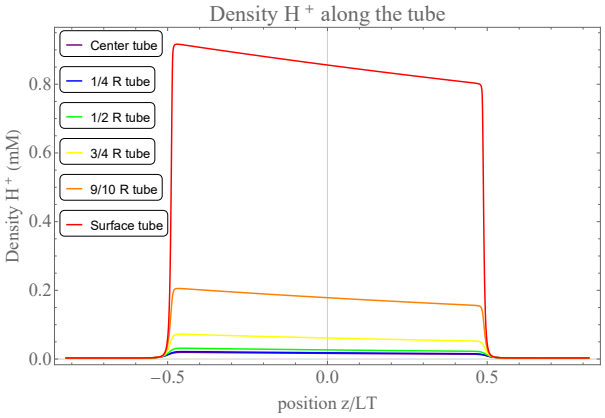

Figure 30: Density of H^+-ions in a tube of length $L = 1250$ m and radius $R = 40$ nm, for an applied concentration drop of 0.1 mM, with viscosity $\eta = 9.544 \cdot 10^{-4}$ Pa s. The surface is charged according to the charge regulation model described in Sec. 2.6.

E Electric current in the non-linear regime

We applied a concentration drop of [0-999] mM with a reference density of 0.1 mM over the tube. We used a regulated surface charge described in Sec. 2.6. The radius R and length L are 40 nm and 1250 nm respectively. We calculated the electric current for a variety of concentration drops. We expected the current to behave as given in Eq. (4.1). The results of the calculations are given for two meshes in Fig. 31 (the second mesh has an improved number of mesh-points by a factor 10). From Fig. 31 we can see that it is hard to analyse the current in this regime of concentration drops, due to the fact that the current is sign-dependent of the concentration drop. When we calculate the total electric current $I_{\text{tot}} = I_{\text{Na}} + I_{\text{Cl}} + I_{\text{H}}$ we can neglect I_{H}, because this current is several orders of magnitude smaller than the currents due to Na^+ and Cl^-. The current which arises from the transport of Cl^- is positive, because these ions are negative and the current is measured in the negative z-direction. We expected the current to be in the same direction as the concentration gradient(negative I), due to the fact that the Na^+-ions would more easily move through the negatively charged nanotube. This is the case for most concentration drops, however for concentration drops around 1 M this is not true. This is an interesting result, which we sadly cannot investigate further due to time restrictions, we concluded from Fig. 31 that this result is not accrue from the mesh, because the changes of the results only slightly depend on the mesh, and if it completely arose from the meshing their would have been more changing results.

F Derivations

F.1 Derivation continuity equation

To derive the continuity equation we first derive the mass continuity equation and afterwards we can generalize this equation. We consider an infinitesimal cube, the mass-flux inward minus the mass-flux outward is equal to the derivative of mass with respect to time: $\dot{m}_{in} - \dot{m}_{out} = \dfrac{\partial m}{\partial t}$, where the dot represents a flux. The sides of the cube are dx, dy and dz, one corner of the cube has position (x,y,z). If we take the flow, with velocity $\mathbf{u} = (u, v, w)$ coming inward from the three planes which touch the corner (x,y,z). The other planes of the cube have an outgoing mass-flux. Then one can write

$$\dot{m}_{in} = \rho u|_x dydz + \rho v|_y dxdz + \rho w|_z dxdy, \tag{F.1}$$

$$\dot{m}_{out} = \rho u|_{x+dx} dydz + \rho v|_{y+dy} dxdz + \rho w|_{z+dz} dxdy, \tag{F.2}$$

$$\frac{\partial m}{\partial t} = \frac{\partial}{\partial t}(\rho dxdydz) = \frac{\partial \rho}{\partial t} dxdydz. \tag{F.3}$$

$$\tag{F.4}$$

Substituting this in $\dot{m}_{in} - \dot{m}_{out} = \dfrac{\partial m}{\partial t}$ and dividing both sides by $dxdydz$. gives

$$\frac{\rho u|_x - \rho u|_{x+dx}}{dx} + \frac{\rho v|_y - \rho v|_{y+dy}}{dy} + \frac{\rho w|_z - \rho w|_{z+dz}}{dz} = \frac{\partial \rho}{\partial t}, \tag{F.5}$$

$$\frac{\partial(\rho u)}{\partial x} + \frac{\partial(\rho v)}{\partial y} + \frac{\partial(\rho w)}{\partial z} + \frac{\partial \rho}{\partial t} = 0, \tag{F.6}$$

$$\nabla \cdot (\rho \mathbf{u}) + \frac{\partial \rho}{\partial t} = 0. \tag{F.7}$$

From this calculations we derived the mass continuity equation:

$$\frac{\partial \rho}{\partial t} + \nabla \cdot \mathbf{J} = 0. \tag{F.8}$$

The mass continuity equation can also be used for other conserved quantities like particle density and particle flux or energy density and energy flux. Therefore we will call it the continuity equation.

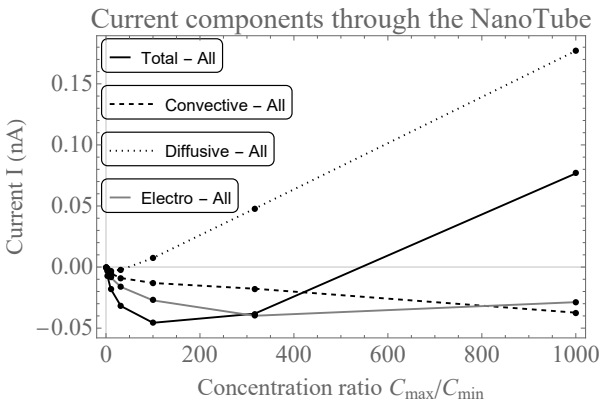

(a) Total I, normal mesh.

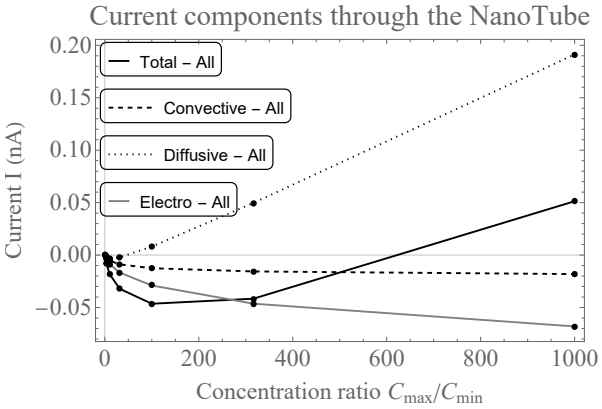

(b) Total I, improved mesh.

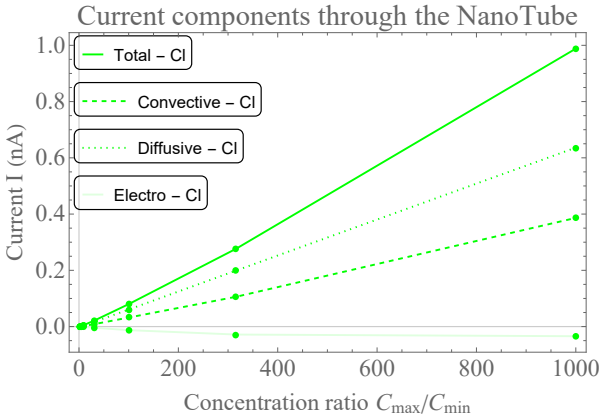

(c) I(Cl^-), normal mesh.

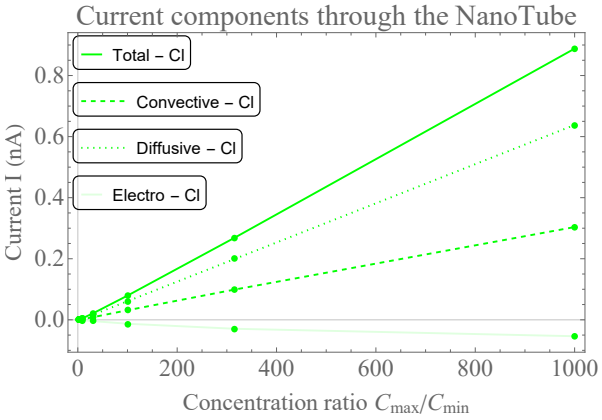

(d) I(Cl^-), improved mesh.

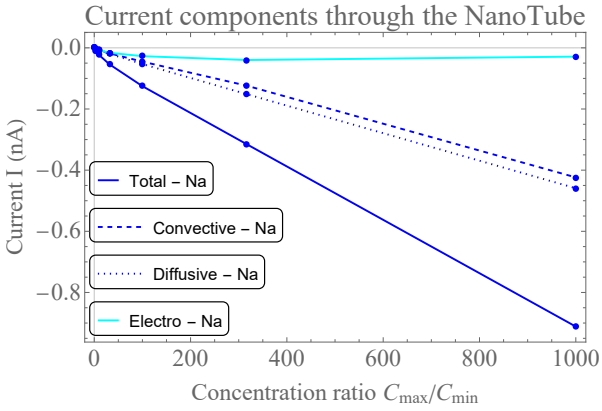

(e) I(Na^+), normal mesh.

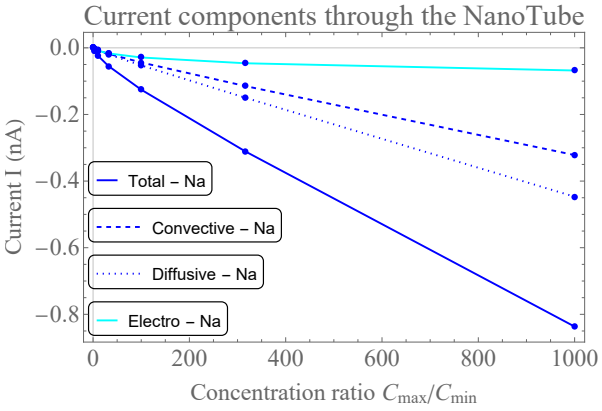

(f) I(Na^+), improved mesh.

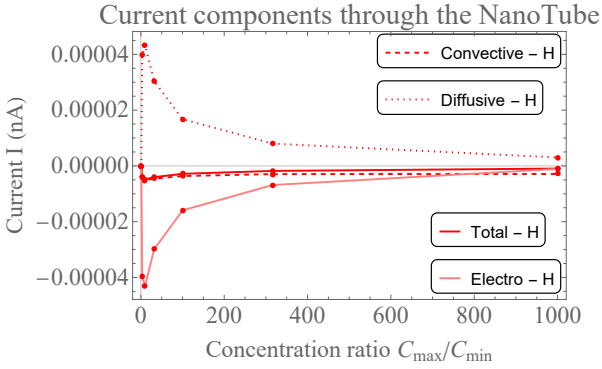

(g) I(H^+), normal mesh.

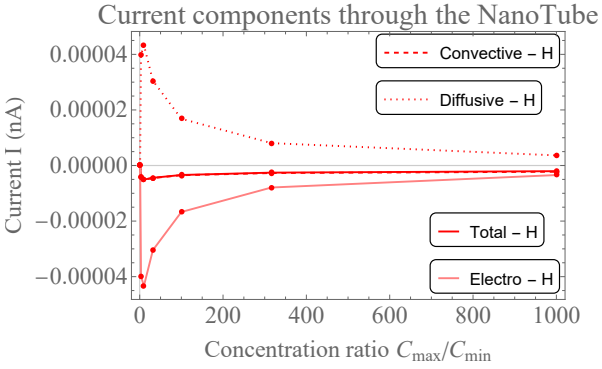

(h) I(H^+), improved mesh.

Figure 31: Current components for all ion species as a result of a concentration drop in a tube of length $L = 1250$ nm and radius of $R = 40$ nm, with viscosity $\eta = 9.544 \cdot 10^{-4}$ Pa s. With diffusion coefficients $D_{Na} = 1.1 \cdot 10^{-9}$, $D_{Cl} = 1.7 \cdot 10^{-9}$ and $D_H = 8.2 \cdot 10^{-9}$ all in m^2/s. For a regulated surface charge as in Eq. (2.19) for $m = 18$ nm^{-2}. Note that the Na^+-ions give rise to a negative current, this is due to the direction of the ion-flow, which is in the negative z-direction.

F.2 Derivation material derivative

For describing the Navier-Stokes equation it is useful to introduce the material derivative, also called the total derivative. The material derivative $\frac{D}{Dt} = \frac{\partial}{\partial t} + \mathbf{u} \cdot \nabla$, where $\mathbf{u}$ is the velocity vector. In the material derivative the first term is the local derivative, also called the Eulerian derivative and the second term comes from the movement of the fluid.[16] To derive the material derivative we consider the vector field $\mathbf{v}$(x,t) at two different times: t (at position $\mathbf{x}$) and t + Δt (at $\mathbf{x} + \Delta\mathbf{x}$), because the quantity of a particle we want to consider has moved by $\Delta\mathbf{x}$ during Δt. Hence

$$\begin{aligned}
\Delta\mathbf{v} &= \mathbf{v}(\mathbf{x} + \Delta\mathbf{x}, t + \Delta t) - \mathbf{v}(\mathbf{x}, t) && \text{(F.9)}\\
&= \mathbf{v}(\mathbf{x} + \Delta\mathbf{x}, t + \Delta t) - \mathbf{v}(\mathbf{x}, t + \Delta t) + \mathbf{v}(\mathbf{x}, t + \Delta t) - \mathbf{v}(\mathbf{x}, t) && \text{(F.10)}\\
&= \frac{\mathbf{v}(\mathbf{x} + \Delta\mathbf{x}, t + \Delta t) - \mathbf{v}(\mathbf{x}, t + \Delta t)}{\Delta t}\Delta t + \frac{\mathbf{v}(\mathbf{x}, t + \Delta t) - \mathbf{v}(\mathbf{x}, t)}{\Delta\mathbf{x}}\Delta\mathbf{x} && \text{(F.11)}\\
&= \frac{\partial\mathbf{v}}{\partial t}\Delta t + \sum_{i=1}^{3}\frac{\partial\mathbf{v}}{\partial x_i}\Delta x_i. && \text{(F.12)}
\end{aligned}$$

If we divide both sides by Δt this results in

$$\frac{\Delta\mathbf{v}}{\Delta t} = \frac{\partial\mathbf{v}}{\partial t} + \sum_{i=1}^{3}\frac{\partial\mathbf{v}}{\partial x_i}u_i, \tag{F.13}$$

where $u_i = \frac{\Delta x_i}{\Delta t}$. In the limit of an infinitesimal time difference it takes the form

$$\frac{D\mathbf{v}}{Dt} = \frac{\partial\mathbf{v}}{\partial t} + \mathbf{u} \cdot \nabla\mathbf{v}. \tag{F.14}$$

Therefore the material derivative is:

$$\frac{D}{Dt} = \frac{\partial}{\partial t} + \mathbf{u} \cdot \nabla. \tag{F.15}$$